Determination of a Predictive Stiffness Model for a 1 DOF Human Inspired Robotic Joint

Michael Boyarsky
Marquette University

DETERMINATION OF A PREDICTIVE STIFFNESS MODEL FOR A 1 DOF HUMAN INSPIRED ROBOTIC JOINT

by

Michael P. Boyarsky, B.S.

A Thesis Submitted to the Faculty of the Graduate School,
Marquette University,
in Partial Fulfillment of the Requirements for
the Degree of Master of Science

Milwaukee, Wisconsin

August 2014

ABSTRACT

ENGINEERING ROBOTIC JOINTS FOR HUMAN-ROBOT INTERACTION

Michael P. Boyarsky, B.S.

Marquette University, 2014

In order to facilitate more natural and intuitive interaction for human users, robots need to move in a more human-like manner as compared to current robots. This change would enable humans to better anticipate robot movements (which would allow humans to better avoid collisions if necessary) and also improve safety in the context of a collision between a robot and a human.

The goal of this thesis was to analyze experimental data of human motion to gain an understanding of how human motion and robot motion differ. From this understanding, a neuro-motor model (NMM) of a human elbow (previously established by Beardsley et al.) was augmented by the addition of a variable stiffness quality. The work in this thesis developed and tested a predictive stiffness model that attempts to recreate the stiffness values used by humans in the context of a disturbance rejection task.

ACKNOWLEDGEMENTS

Michael P. Boyarsky, B.S.

TABLE OF CONTENTS

TABLE OF CONTENTS — *Continued*

TABLE OF CONTENTS — *Continued*

TABLE OF CONTENTS — *Continued*

LIST OF FIGURES

LIST OF FIGURES — *Continued*

CHAPTER 1

Introduction

1.1 Introduction

As environments shared by humans and robots become increasingly prevalent, the need for robots to move like humans also increases, so that humans can better anticipate robot movements. Current industrial robots are designed for fast, repetitive, and precise movements [3, 4], while human movements are smoother and more compliant. This causes interactions in environments shared by humans and robots to be awkward and potentially dangerous [5]. In order to facilitate more natural and intuitive interaction for human users, robots need to move in a more human-like manner [6–8]. This change would enable humans to better anticipate robot movements (which would allow humans to better avoid collisions if necessary) and also increase the compliance of the robotic joints, which would improve safety in the context of a collision.

The goal of this thesis was to analyze experimental data of human motion to gain an understanding of how human motion and robot motion differ. From this understanding, a model of how to recreate this motion in the context of a human-like joint in a robot was developed and tested.

1.2 Problem Statement and Literature Review

At this time, the general approach to developing robots for human environments is to adapt commercially available robots for human interactions [9, 10]. To adapt a robot in this way, the robot is typically given trajectories that closely mimic human movements [11, 12]. While this approach often successfully creates the appearance of human motion, this approach does not create functionally similar motion to humans.

Pollard, et al. adapted the motion of human subjects to a humanoid robot by way of trajectory tracking [13]. This work involved tracking the movements of

seven human actors through a series of designated moves. After the angular trajectories were determined and mapped to robotic joint trajectories, the robot was able to reproduce the motion of the human subjects. This work successfully exhibits a demonstration of a robot that can successfully create the appearance of human motion. However, it is important to note that this demonstration retains all of the dynamic and control qualities of the robot; the motion only appeared human and did not functionally mimic the way the human subjects created the motion. One hypothesis of this thesis is that one of major aspects of human motion that this approach fails to capture is compliance in the context of a disturbance rejection task.

Many other groups have studied ways of using stiffness/impedance to control robots. The theoretical basis for using impedance control is well-understood [14, 15] and has been directly implemented using industrial robots [16]. This differs from the trajectory matching approach used in the previous paragraph because this approach does not try to recreate human motion, but rather it attempts to move a robot in a way that can yield to the surrounding environment. Impedance control has also been applied to human-robot interaction (HRI) [17] and the effects of mechanical impedance control as they relate to human perception has been studied in the context of robots [18]. More recently, Hirzinger et al. have used partial impedance control methods to improve the performance of robots in the context of environments shared with humans [19]. While these methods have demonstrated "softer" robots as compared to some other methods, current impedance control methods are not designed to make robots mimic the type of impedance demonstrated by humans.

Variable stiffness joints would enable the implementation of impedance control in robots. Different variable stiffness joints have demonstrated the ability achieve stiffness values in the range of 30 N/m to 2700 N/m, specifically in the context of robots [20–22]. These types of joints are relevant to this work because if the predictive model developed in this thesis were to be properly implemented, it would require variable stiffness joints. Since these joints have been demonstrated, the prospect of implementing the predictive stiffness model developed in this thesis is possible.

To create a robot suited for HRI, it is useful to have metrics to assess how

well a robot performs in the context of HRI. Steinfeld et al. documented ways of assessing a robot's performance in an HRI setting by describing different broad metrics for HRI [23]. The work in this thesis focuses on the metrics of 'obstacle encounter,' 'interaction characteristics,' and 'subjective ratings.' By adding a predictive stiffness control model, the intensity of collisions is severely reduced, thus improving a robot's 'obstacle encounter' performance. Consequently, the robot's 'interaction characteristics' are also improved by decreasing the severity of a collision. Furthermore, by embodying a more human-styled motion, the movements of the robot are more predictable, intuitive, and easy to interact with for humans, thus theoretically improving the robot's 'subjective ratings.'

The work presented in this thesis has identified disturbance rejection as an important characteristic of motion where humans and robots largely differ. Human joints are compliant and reactive; when they encounter an unexpected disturbance in the way of a movement, they do not "power" through it, like robots do. In order to build a robot that can properly interact with humans, human disturbance rejection behavior must be captured by a robot that is intended to interact with humans in a shared environment [5, 24, 25]. Current robots fail to capture the variable motion parameters that are modulated by humans in the context of a disturbance [26]. This thesis demonstrates an understanding of a variable stiffness quality present in humans that dramatically affects a robots ability to move like a human in the context of a disturbance rejection task.

Many groups have used robots to reproduce human trajectories and even applied impedance control to do so [13, 19]. While impedance control has been applied to robots, these attempts have been focused on general ideas, such as making robots "softer," rather than being focused on trying to emulate how humans use variable stiffness to control their joints [25]. Furthermore, there has not been an attempt to use such an understanding to develop a predictive stiffness model that mimics human joint control to recreate robot motion that is functionally similar to human motion. The work in this thesis develops and demonstrates a predictive variable stiffness model (a model that uses the available input parameters to predict what the stiffness value a human would have produced in the same situation). A robot that used this predictive stiffness model would better emulate human motion

and consequently be better suited for HRI.

To develop the predictive stiffness model, experimental data was taken from human subjects restricted to the use of their elbow as a 1 DOF joint. The data from the human subject testing was then used to develop a neuro-motor model (NMM) that captured the dynamics and control of a human elbow. The NMM was then used to optimize a time-varying, discrete, variable stiffness, $k(t)$, that improved agreement between the model and the data in the context of a disturbance rejection task. From the optimized $k(t)$, a predictive stiffness function was synthesized, using motion parameters such as angular position (θ), angular velocity (ω), etc. as inputs. This sequence is described below in Fig. 1.1.

Step 1	Step 2	Step 3	Step 4

Experimentally Measure Human Elbow Motion Behavior	Develop Neuro-Motor Model (NMM) to Embody Recorded Human Motion Data	Optimize Stiffness k(t) to Improve NMM Performance for Disturbance Rejection	Create Predictive Stiffness Model to Emulate Human Joint Behavior
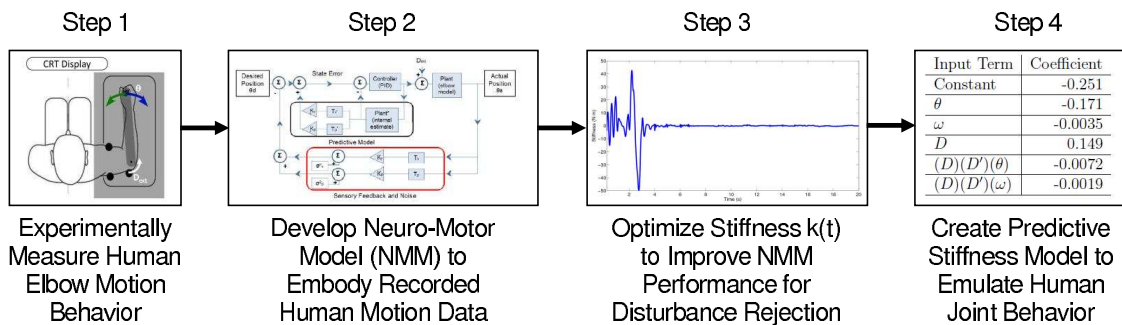
Figure 1.1: Development Sequence for Predictive Stiffness Model

Note that the above steps are further described in the corresponding sections: experimental data and NMM - Chapter 2, optimized stiffness - Chapters 3 and 4, predictive stiffness model - Chapter 5.

1.3 Outline of Thesis

To document the different aspects of the work presented in this thesis, a short outline follows.

1.3.1 Neuro-Motor Model

Chapter 2 presents the NMM of a human elbow that was developed to analyze and capture human motion so that it could be compared to robot motion. This was initially developed by Beardsley et al. and includes the plant dynamics, control system, and feedback loop that humans are believed to use [1, 27]. The

disturbance rejection task was identified through the NMM as a motion task in which the agreement between the NMM and experimental data could be most improved.

1.3.2 Time-Varying Parameters

Chapter 3 presents an investigation into adding a time-varying quality to different model parameters in the NMM to improve the agreement between the model and the experimental data in the context of the disturbance rejection task. Ultimately, the NMM response was most improved by adding variable stiffness as compared to the other model parameters.

1.3.3 Variable Stiffness

Once variable stiffness was identified as the most important parameter for improving the NMM response in the context of the disturbance rejection task, a variable stiffness with a unique value at each time step, $k(t)$, was determined. Chapter 4 presents the methods used to optimize $k(t)$ to minimize the error between the NMM response and the experimental data in the context of a disturbance rejection task, while maintaining performance in a step input task.

1.3.4 Predictive Stiffness Models

Chapter 5 presents the development of predictive stiffness models based on the optimized stiffness vector $k(t)$, as determined in Chapter 4. A predictive model was developed to create a function $k(\theta, \omega, etc.)$ that could determine the optimal stiffness value at a given time based on the available input parameters. This stiffness model would enable a robot to use the stiffness value that a human would use in the same situation, rather that use values that are more typically used by industrial robots.

1.3.5 Experimental Verification

Chapter 6 presents an experimental implementation of the predictive stiffness model described in Chapter 5. The experimental setup involved a motor, with a 'forearm' mass, which was tested through a step response task and a continuous

torque disturbance rejection task. The model responded in manner consistent with the predictions of the NMM. These results provide evidence that using the predictive stiffness model described in Chapter 5 would result in the performance expected by the NMM.

1.3.6 Conclusions and Potential Applications

Chapter 7 discusses the conclusions and prospective applications for the work presented in this thesis. This includes potential applications and areas of the work presented in this thesis that could be expanded in future projects.

CHAPTER 2

Neuro-Motor Model Development

2.1   Introduction

To develop a robot intended for human interaction, the characteristics that most differentiate human motion from robot motion were identified. Beardsley, et al. had previously described human motion by developing a neuro-motor model (NMM) in Matlab Simulink that is consistent with their experimental data from normal human subjects [1]. This model was developed to match experimental subject data in various contexts including disturbance rejection and step input.

In theory, if the aspects of human motion can be captured by the NMM, they could subsequently be reproduced and demonstrated by a robot. Consequently, a large part of this research was dedicated to developing the model and improving performance in the context of tasks, namely step input and disturbance rejection, that would be important for human-robot interaction (HRI).

2.2   Human Subject Information

2.2.1   Step Response Trials

Data was collected from twelve subjects. Written informed consent, in accordance with the institutional guidelines approved by Marquette University, was obtained from all subjects prior to the task. Subjects ranged in age from 22 to 75 years old.

2.2.2   Disturbance Rejection Trials

Data was collected from two subjects. Written informed consent, in accordance with the institutional guidelines approved by Marquette University, was obtained from all subjects prior to the task. Subjects ranged in age from 23 to 27 years old.

2.3   Experimental Data

In developing the NMM, human subject data was recorded [1, 27]. The subjects performed two main tasks: a visual step input task and a disturbance rejection task. Both tasks involved the subject in the environment described in Fig. 2.1. This configuration restricts the subject to the 1 degree-of-freedom use of only their right elbow as seen in Fig. 2.1. The subject grabs the handle, which is attached to a robotic lever. The lever is attached to a motor, which can act passively or apply a torque disturbance. The system has an encoder to measure the motion imparted by the human subject. For the step input task, the subject was tasked with maintaining a cursor on a target, which was instantaneously moved from $\theta = 0$ to $\theta = \theta_{step}$ at $t = t_{step}$ on the screen as shown in Fig. 2.1. The cursor was a circle, that is intended to surround the target, which was a bullseye. Both were moved horizontally across the screen, where the horizontal position of the cursor was mapped to the angular position, θ, of the handle. Data from twelve subjects who had participated in the step response experimental activity was analyzed. For the disturbance rejection task, the subject was asked to maintain a cursor at $\theta = 0$ while a continuous torque disturbance, D_{ext}, was applied to the handle which was pivoted at the elbow. For the disturbance rejection task, data was collected from two subjects, with ten trials of data per subject.

2.3.1   Step Input Instructions

The instructions given to human subjects before conducting the step response task were, "The target will randomly appear to your left or your right on the screen. Move the cursor to the target as quickly and as accurately as possible."

2.3.2   Disturbance Rejection Instructions

The instructions given to human subjects before conducting the disturbance rejection task were, "The robot will apply gentle forces to your hand, pushing it away from the center. Your goal is to bring your hand back to the center as quickly and accurately as possible. Try not to stiffen your elbow and resist movement, but rather let the robot move your hand and then make corrections."
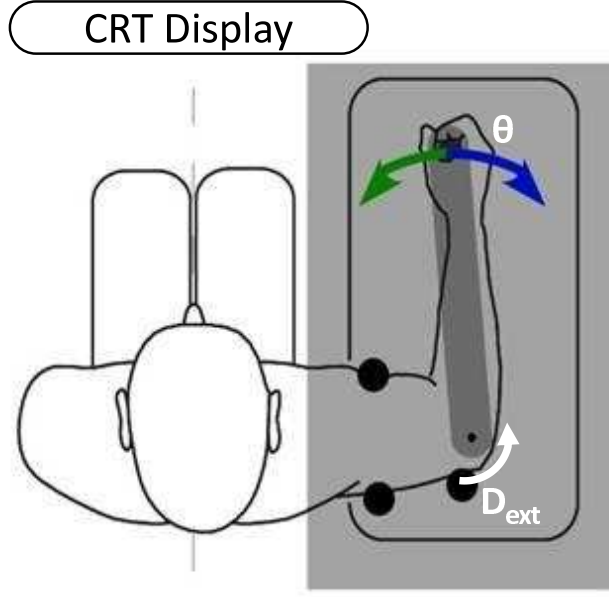
Figure 2.1: Diagram of Experimental Setup for Step Input and Disturbance Rejection Tasks (adapted from [1])

2.4   NMM of Human Elbow

Fig. 2.2 shows the overall block diagram for the NMM as developed by Beardsley et al. [1,27]. The feedback loop can be seen as having a proprioceptive and a visual component as shown in Fig. 2.3. The internal predictive model surrounds the PID controller and negates ill-effects that result due to visual and proprioceptive delays present in the human sensing system. The disturbance, D_{ext}, is added to the model before the plant, which is outlined in Fig. 2.4. Last, the NMM angular error, θ_{Error}, is calculated by Equation 2.1. A more specific description of the components of the NMM is included in the following sections.

$$\theta_{Error} = \sum_{i=1}^{i_f}(\theta_{NMM}(i) - \theta_{Data}(i))^2 \tag{2.1}$$

where i represents an index corresponding with a time step and i_f represents the final time step in a given trial.

To apply this model to a different joint system, a different plant would have to be used. Additionally, the control gains, feedback gains and delays, predictive plant model, and other joint-specific parameters would have to be optimized to fit
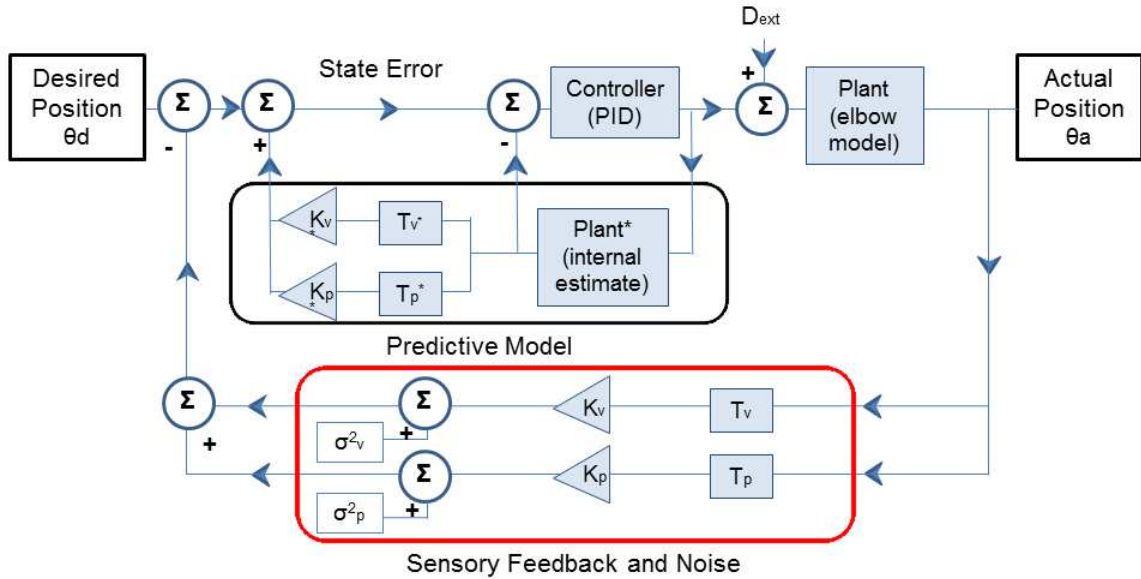
Figure 2.2: Neuro-Motor Model for a Controlled Human Elbow (adapted from [1])

experimental data. Stiffness and damping of those joints would have be modified to fit the joint. When this model is applied to different subjects, these parameters also must be fitted to the experimental data to obtain the subject-specific values.

2.4.1 Controller

The control system of the NMM is represented by a classical PID controller. While a PID controller is a simplification of an actual human control system, a PID controller was demonstrated to be an accurate representation of a human control system [1, 27].

2.4.2 Feedback System

The feedback system of the NMM, is based upon a model of a human's posture system, seen in Fig. 2.3 [2]. This model mixes visual feedback, proprioceptive feedback, and graviception to form the closed loop and includes time delays to account for sources of delay in signal processing such as conduction delays, processing delays, and excitation/activation delays. Different biological systems weight visual and proprioceptive feedback differently and thus the gains are adjusted depending on the task. In the context of the elbow system, the proprioceptive feedback is weighted heavier, with a gain $w_p = 0.7828$ (K_p in Fig.
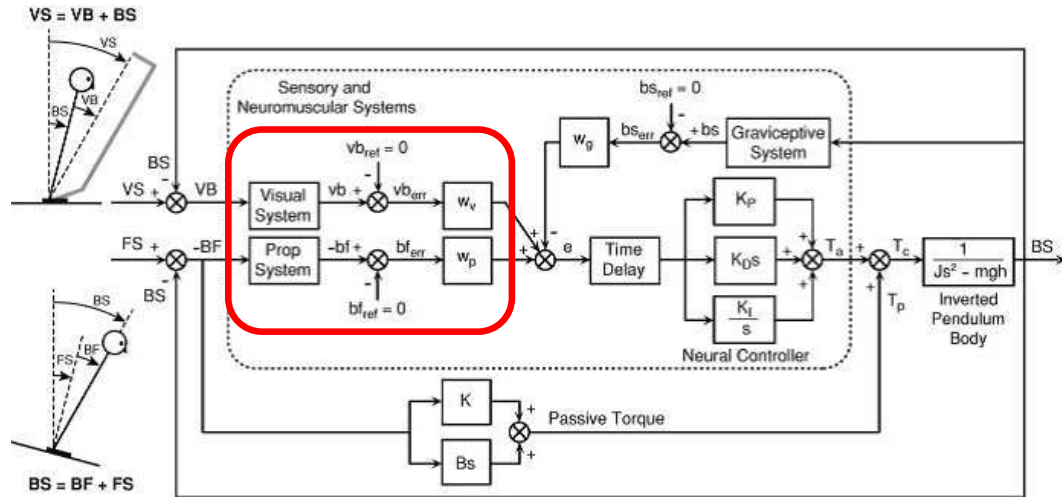
Figure 2.3: Human Feedback System (adapted from [2])

2.2), while the visual feedback has a gain $w_v = 0.2172$ (K_v in Fig. 2.2).

2.4.3 Internal Predictive Model

Human sensing is delayed for a variety of reasons. Visual feedback delays human reactions by approximately 300-450ms while proprioceptive feedback delays reactions by approximately 140-200ms [27]. These delays would make the feedback loop very ineffective for properly controlling human processes. However, humans have an internal, predictive model that enables the brain to anticipate the results of commands that the brain issued to a certain joint system, which is included as part of the NMM [1, 28]. This enables the human to circumvent the delays and virtually negate any inhibiting effects the delays would incur.

2.4.4 Plant Dynamics

The dynamics of the elbow/wrist system were modeled in SimMechanics, generation 2 (see Fig. 2.4). The components of the elbow system (upper arm, forearm, and hand) were modeled as inertial bodies in SimMechanics and joined at the elbow. The average values for masses, lengths, and inertial matrices were used from the report by Chandler, et al. [29]. The wrist was treated as a fixed joint. From this model, a torque was applied to the elbow joint, which experiences stiffness (K(t) in Fig. 2.4) and damping (B(t) in Fig. 2.4) about the 1 DOF revolute joint.

It is important to note that the modeling of the stiffness and damping of the
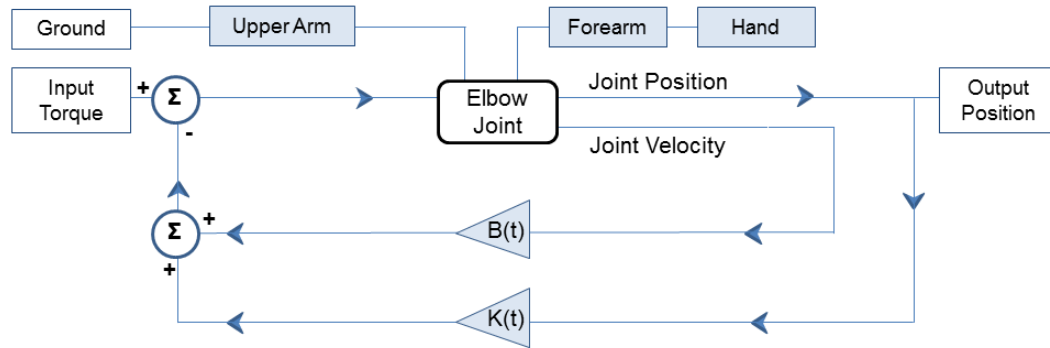
Figure 2.4: Plant Dynamic System for a Human Elbow

elbow are not typical joint stiffness and damping that would be experienced in a mechanical joint/system. Rather, they represent an "effective stiffness" and "effective damping" that represent the resultant behavior of the joint that occurs when a human contracts muscles on either side of the joint. The human is not actively controlling specific stiffness or damping parameters that are part of the motion that is desired. The human is contracting different numbers of muscle fibers on either side of the joint and depending on the muscle behavior, the joint consequently experiences "stiffness" and "damping" in a similar manner to that of traditional mechanical joints. The stiffness and damping values discussed and used in the NMM represent these "effective" values. If a robot were to embody this model, it would be able to simply produce these values naturally and would ignore the "effective" nature of these parameters presented here.

To properly account for human subject sizes, a scaling factor was applied to properly account for subjects of different sizes. A length scaling factor was applied to the dimensions of the upper arm, forearm, and hand and a mass scaling factor was applied to the masses of those links.

2.5 Modeling Assumptions

In modeling the human elbow system with the NMM, many simplifying assumptions had to be made. Some of these are discussed within the specific related sections in Section 2.4, but will also be described here for clarity. The most significant assumption of the NMM is that the elbow is a 1 DOF joint. In actuality, the human elbow is a multi-DOF joint capable of many types of movements.

However, in the context of the human subject testing, the upper arm is assumed to be fixed and parallel to the ground, resulting in a near 1 DOF joint about an assumed fixed rotation point in the elbow. The wrist was treated as a fixed joint, with the hand parallel to the forearm. The motion of all tasks is assumed to be within the range of motion capable by the subject; the task requirements do not push a subject outside of his/her natural range of motion.

Despite the fact that the NMM has the capacity to account for many of the system delays present in human motor control, all delays aside from the feedback delays were set to zero. The delays were set to zero to enable the optimizer (as discussed in Chapter 4) to perceive a direct correlation between any changed parameters at $i = n$ and the NMM response at $i = n$. The predictive plant model of the NMM, as discussed in Section 2.4.3, was assumed to be perfect.

Two major assumptions were made regarding the inertia of the system. First, the inertia of the subjects was not directly analyzed or measured and an approximation based on subject height was applied. Additionally, the inertia of the handle system (as shown in Fig. 2.1) was not included.

2.6 NMM Performance

Since the NMM is based on measured characteristics of the human body, the model performs reasonably well in most tasks. The differences between the model response and experimental data derive from two main sources: model oversimplification and variance. Some aspects of the NMM are known to be simplifications (e.g., the wrist as a fixed joint). Other aspects of the NMM fail to fully replicate human motion behavior due to missing complexities of human motion that are not fully understood. Stiffness and damping are two characteristics of motion that humans are known to vary across tasks [26]. Variance also plays a large role in modeling humans due to the differences that appear not only between different human subjects, but also between different trials of the same subject. This variance in response introduces difficulty when creating a model designed to match experimental data across multiple trials and multiple subjects.

2.6.1 Step Response Performance

The NMM matches experimental human data for a visual step input. In this task, subjects were asked to keep a cursor on a target, which instantaneously moved on a screen to simulate a step input. For different subjects, the data has a slightly different response. For these subjects, model parameters such as damping coefficient, stiffness, control gain, etc. can be adjusted as constant parameters to properly match the experimental data and variations between subjects can be properly accounted for by adjusting model parameters. Fig. 2.5 demonstrates an example of the agreement between the model and the experimental data for one representative subject. Normalized angular position represents $\theta_{Measured}/\theta_{Step}$ so that trials with different step magnitudes and directions can be compared.
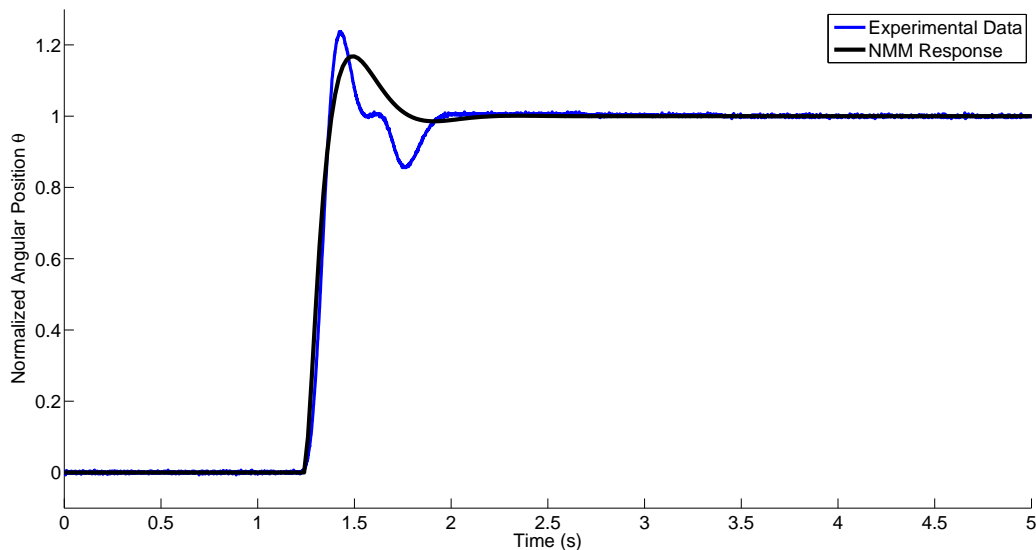
Figure 2.5: Step Response for Human Subject Experimental Data and NMM Predicted Response

2.6.2 Disturbance Rejection Performance

Subjects also performed a disturbance rejection task in which they were required to dynamically maintain the position of a cursor while a time-varying torque disturbance (D_{ext} in Fig. 2.2) was applied to the handle. When a disturbance was applied to the model, the error between the model and the data was larger as compared to the error for the step input task, seen in Fig. 2.6. The
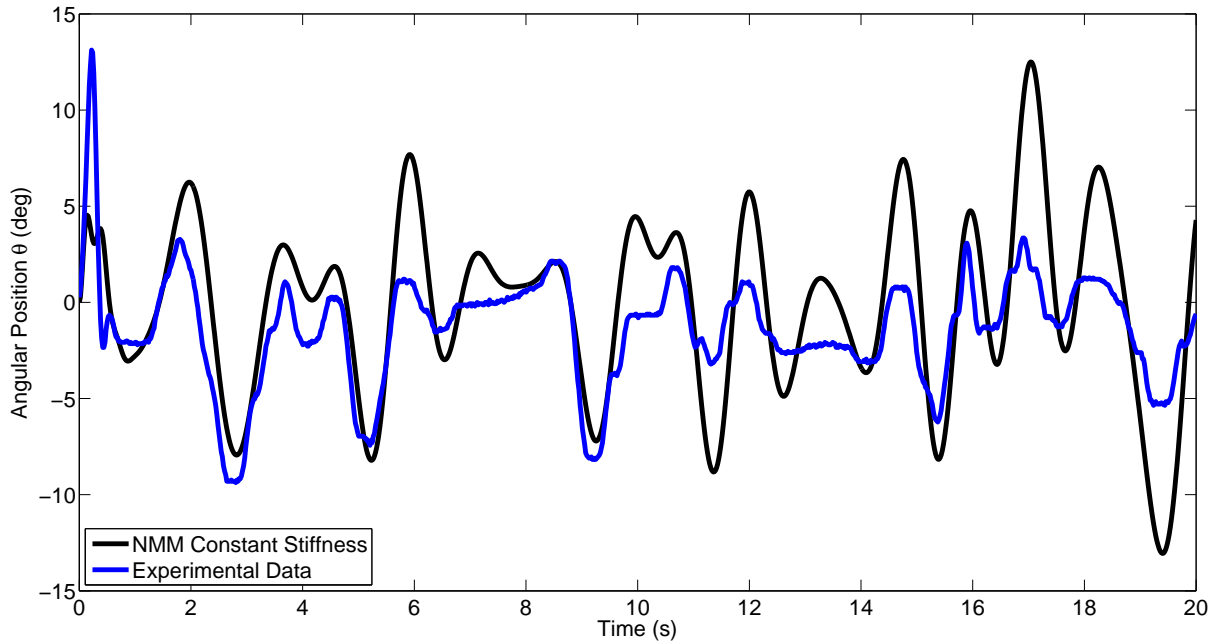
Figure 2.6: Disturbance Rejection for Human Subject Experimental Data and NMM Predicted Response

disturbance that was applied during this trial is shown in Fig. 2.7.

To improve the performance of the NMM in the context of the disturbance rejection task, it was hypothesized that adding a time-varying quality to some of the model parameters such as stiffness, damping, or control gains would improve the model performance for this task. This hypothesis was based upon the fact that human joints vary these quantities continuously depending on the desired motion [26]. It was further hypothesized that the variable quality that these parameters experience is directly related to the disturbance.

2.7   Conclusion

The NMM discussed in this chapter captures many aspects of human motion, including the plant dynamics of a human elbow system, the control system used by the brain to maintain a desired trajectory, the delays present in the human sensing system, the internal predictive model used to offset the ill-effects of sensing delays, and the visual and proprioceptive feedback components associated with the human feedback loop. This model currently matches experimental data well for a step
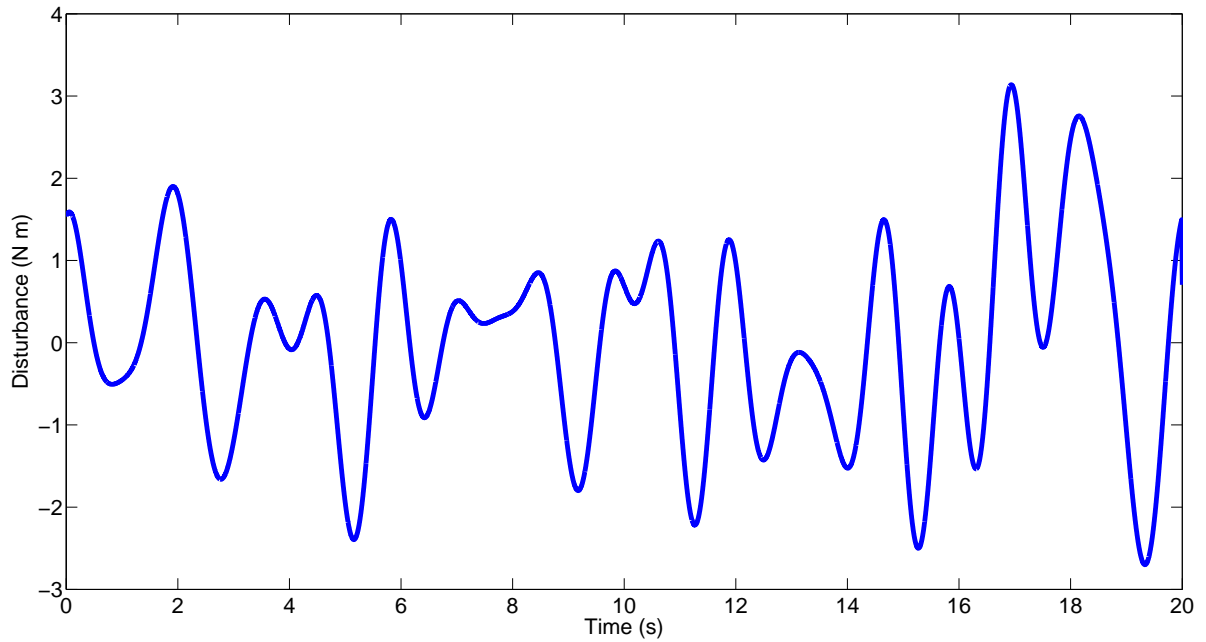
Figure 2.7: Continuous Torque Disturbance (D_{ext}) for Subject 2, Trial 1

input. Introducing a time-varying parameter will be investigated, as described in Chapter 3, in order to improve the NMM agreement in the context of a disturbance rejection task.

CHAPTER 3

Time-Varying Parameters

3.1   Introduction

If a relationship between the input parameters (θ, ω, disturbance, etc.) and a time-varying parameter could be determined, a predictive model for that time-varying parameter could be synthesized. This predictive model would ideally mimic human joint behavior in a given circumstance defined by the available input parameters. If this type of predictive model were implemented with a robot, that robot would be capable of predicting how to vary such a parameter and would thus have the capacity to emulate that aspect of human motion. Using a predictive model would thereby demonstrate motion that is more human-like as compared to robots that do not capture this aspect of human motion.

This chapter discusses a data-driven approach to determining which parameters within the neuro-motor model (NMM) described in Chapter 2 are the best candidates to exhibit a time-varying quality in order to improve the match of the NMM to the experimental data. After investigating the different available parameters, stiffness was observed to be the most crucial variable needing to exhibit a time-varying quality in order to reduce the error between the experimental data and the NMM in the context of a disturbance rejection task.

3.2   Time-Varying Parameters

To improve the agreement between the NMM and the experimental data, control gain, damping, and stiffness were tested as time-varying parameters. This investigation tested the hypothesis that adding time-varying qualities to any or all of these parameters was necessary to properly capture human performance in the context of the disturbance rejection task described in Section 2.3. The goal of this investigation is to determine which parameter, when treated as time-varying, affects the model response in the context of a disturbance rejection task the most. To

determine this parameter, a sensitivity test was performed on each of the parameters.

This investigation was conducted in a "one-factor-at-a-time" (OFAT) manner due to the fact that simultaneously optimizing multiple variables proved to be too computationally intensive for the available resources. Despite the fact an OFAT approach limits the ability of an optimizer to properly account for interactions between multiple time-varying parameters, it still provided usable results that accomplished the desired goals of the project. Further discussion of some limitations of only optimizing the most sensitive parameter, stiffness, can be found in Section 4.5.

For this investigation, the data taken from subject two, trial two from the disturbance rejection task was used. This trial is representative and was chosen due to the fact that it had a peak in the angular error early in the trial, which was a good place to test the sensitivity of model parameters as time-varying.

3.2.1 Variable Control Gain

When the control gains were varied, there was little change in the model response. This result lead to the conclusion that the control gains were not a parameter that benefitted from a time-varying quality to improve the model. In this
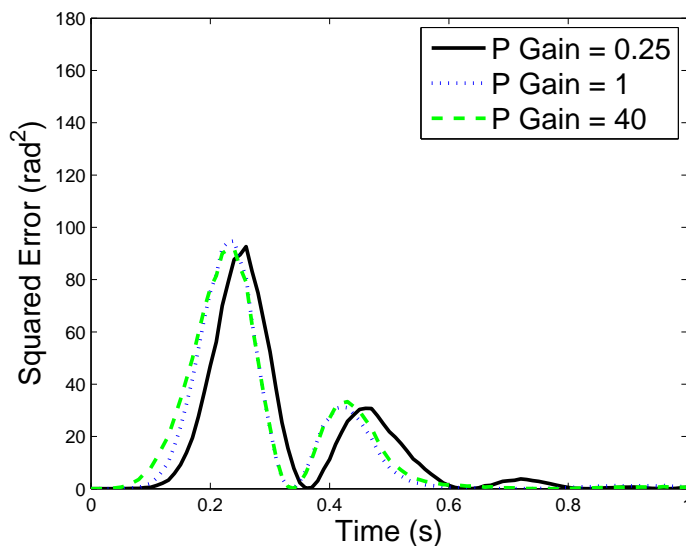
Figure 3.1: Model Error for Different Control Gains (Subject 2)

test, the gains were varied between 0.25 and 40, outside of which the system is unstable. For reference, a plot of the error between the model and the data based on different control gains for subject 2, trial 2, can be found in Fig. 3.1. This plot demonstrates the system sensitivity to a varying control gain as it affects the NMM performance in the context of a disturbance rejection task. The results of this investigation indicated that while it was important to use a control gain that provided stability for the system, the magnitude of the control gain does significantly vary the model performance in the context of the disturbance rejection task.

3.2.2 Variable Damping

When the damping coefficient (B(t) in Fig. 2.4) was adjusted, the model behavior exhibited some change in response that seemed to correlate to what would be an adjustable parameter that would improve model performance. The adjustment of the damping coefficient was applied simultaneously to the internal predictive plant model, in addition the actual plant. This result led to a similar conclusion as the control gain, however, which was that damping is not a parameter that needs to be time-varying to properly emulate human motion with the model. The error between the model and the experimental data for different damping
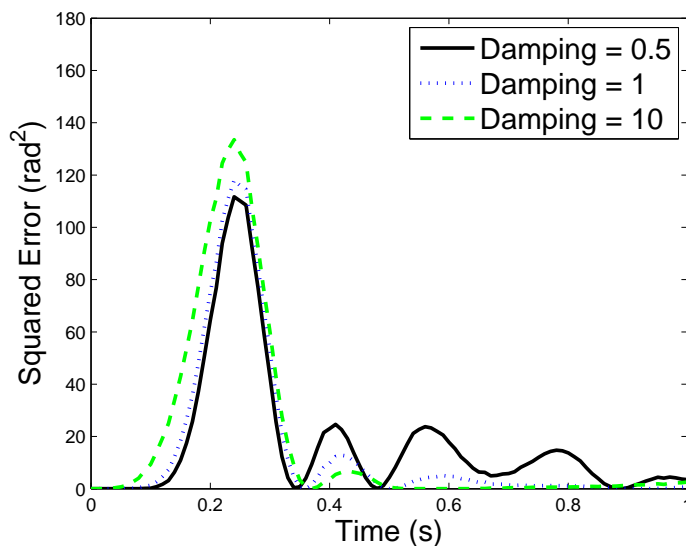
Figure 3.2: Model Error for Different Damping Coefficients (Subject 2)

values can be seen in Fig. 3.2. This plot demonstrates the system sensitivity to a varying damping coefficient as it affects the NMM performance in the context of a disturbance rejection task. The results of this investigation indicated that the damping coefficient, similar to the control gains as discussed in Section 3.2.1, were necessary for stability, but does not significantly vary the model performance in the context of the disturbance rejection task. This conclusion was revisited, however, when it was noticed that applying a time-varying damping coefficient can "enable" a time-varying stiffness to be more impactful in some contexts of the disturbance rejection task.

3.2.3   Variable Stiffness

When the stiffness value was varied, there was a direct difference in response which correlated with the value of the stiffness used. The adjustment of the damping coefficient was applied simultaneously to the internal predictive plant model, in addition the actual plant. There was a large difference in model output that correlated with the stiffness value used, which lead to the conclusion that a time-varying stiffness had the most potential to significantly impact the model response in the context of the disturbance rejection task. This result is demonstrated in Fig. 3.3. This plot demonstrates the system sensitivity to a
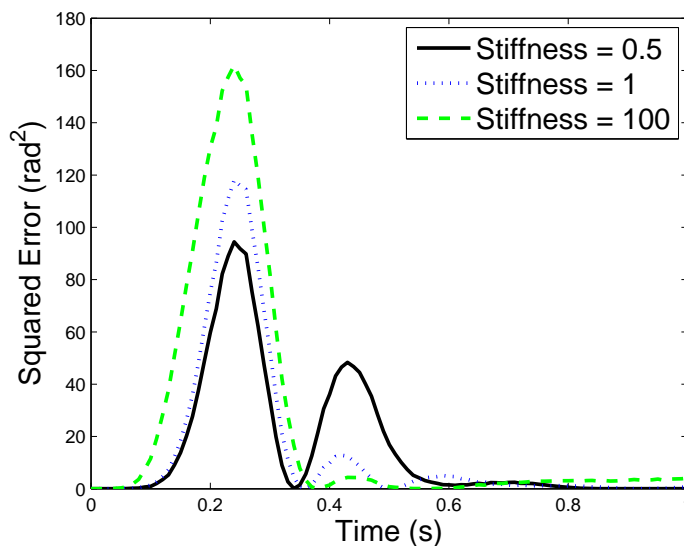
Figure 3.3: Model Error for Different Stiffness Values (Subject 2)

varying stiffness as it affects the NMM performance in the context of a disturbance rejection task.

3.3   Conclusion

As evidenced by Fig. 3.1, Fig. 3.2, and Fig. 3.3, stiffness was the model parameter that provided the most sensitivity for the NMM in the context of a disturbance rejection task. While this investigation was not exhaustive, it provided a starting point for an investigation in the application of a time-varying parameter to the NMM. These results could also be lacking with respect to other tasks. This result provided evidence that implementing a time-varying or predictive stiffness model would have the most effect on the NMM response, as compared to other parameters, and have the highest capacity for improvement, with respect to the error between the NMM and the experimental data for the disturbance rejection task. It was hypothesized from this result that time-varying stiffness was an important aspect of human motion to capture in order to improve the disturbance rejection response of the NMM.

CHAPTER 4

Variable Stiffness

4.1 Introduction

Including a time-varying stiffness quality as part of the robotic joint architecture (see Section 3.2) shows the potential to create the desired human-like motion described in Chapter 1. In order to apply a variable stiffness quality to a robotic joint, a function $k(\theta, \omega, etc)$ must be established that is able to predict the stiffness value that a human would use. To establish such a function, a discrete stiffness vector, $k(t)$, was determined, by way of optimization, that minimizes the sum of the squared angular error between the model response and the experimental data at each point in time. This stiffness vector represents approximately what the human subjects in the corresponding trials used when faced with the disturbance rejection task. From an optimized stiffness vector, a function $k(\theta, \omega, etc)$ can be established, as will be described in Chapter 5.

4.2 Optimizing Variable Stiffness

Stiffness was determined, in Chapter 3 to be the quality that, if made to be time-varying, could most affect the NMM response for disturbance rejection. A time-varying stiffness vector for disturbance rejection was determined by optimization. The optimization minimized the sum of the squared angular error between model and experimental data (from subject 2, trial 2) while changing discrete stiffness values in a variable stiffness vector. This optimization is shown in Equation 4.1, in which θ_{NMM}(angular position of the NMM) is, in part, a function of stiffness. Stiffness was restricted to values typically exhibited by humans, including the possibility for negative stiffness, in cases where humans add energy to a joint system to achieve better performance [26]. Negative stiffness is further discussed in Section 4.2.2.

To create a model for variable stiffness, discrete stiffness values for each time

step were optimized so that the angular position of the model matched the angular position experimental data. To ease the computational demands, the data was down-sampled from t=0.001s to t=0.02s. Decreasing the frequency of time steps did not significantly affect the response of the model, which was verified by comparing the angular position, velocity, and acceleration, as well as the input disturbance, disturbance derivative, and disturbance second derivative before and after decreasing the frequency of time steps.

$$min \qquad f = \sum_{i=1}^{50}(\theta_{NMM}(i) - \theta_{Data}(i))^2 \qquad (4.1)$$

$$t = \frac{i}{50} \; s \qquad (4.2)$$

4.2.1 Interval Size

Ideally, the optimization routine would be applied to a full trial of data (20s), but that length proved too complex from a computational perspective. To alleviate the computational concerns, the solver was applied to smaller intervals of the trials. Intervals ranging from 0.25s to 5s were attempted and intervals of 1s were used based on computation time and success. This interval size represents 50 time steps (t=0.02s), with 20 intervals over each trial.

4.2.2 Upper and Lower Bound Constraint

A lower bound and upper bound were placed on the stiffness values to limit the optimizer to a range of 100 N m to -50 N m (shown in Equation 4.3), which represents approximate values for the extremes that are achievable by humans. Typical relaxed stiffness values for humans fall within a range of approximately 0.5 N m to 5 N m [30]. Negative stiffness values represent when a human puts energy into a joint system. The reason that negative stiffness values are used, instead of restricting the bounds to 0, is to maintain the OFAT approach. That is, in actuality, negative represents an opposite controlled signal, applied to a positive stiffness joint. By using negative stiffness, the optimizer can achieve the desired response by changing the stiffness value, rather than simultaneously having to

change stiffness and control gain.

$$-50Nm \leq k(i) \leq 100Nm \qquad i = 1, 2, ..., 50 \tag{4.3}$$

4.2.3 First Derivative Constraint

Since some results from optimization demonstrated very strong agreement between the model and the data, but produced unphysical stiffness values in which the stiffness versus time curves alternated instantaneously between the bounds of the optimizer repeatedly. In reality, a human cannot change the stiffness of a joint by that magnitude that fast. To apply additional constraints so that the optimizer would produce more physical and achievable stiffness versus time curves, a restriction was applied to the first derivative of the stiffness curve, as seen in Equation 4.4. This constraint forces the optimizer to only vary $k(i)$ by $k(i-1) \pm k'$.

$$|k(i) - k(i-1)| < k' \tag{4.4}$$

where k' represents the constraint value on the first derivative. Note that the specific value of k' is related to the time step and was adjusted as the time step was determined. This constraint can be further expressed by breaking it into a pair of equations, seen in Equations 4.5 and 4.6.

$$k(i) - k(i-1) < k' \tag{4.5}$$

$$k(i-1) - k(i) < k' \tag{4.6}$$

Equations 4.5 and 4.6 can further be expressed as matrices as seen in Equations 4.7 and 4.8, respectively, which are directly compatible with the solver which applies constraints as $Ax < B$.

$$\begin{bmatrix} 1 & -1 & 0 & \cdots & 0 \\ 0 & 1 & -1 & \cdots & 0 \\ \vdots & \vdots & \vdots & \ddots & \vdots \\ 0 & 0 & \cdots & 1 & -1 \end{bmatrix} \begin{bmatrix} k(1) \\ k(2) \\ \vdots \\ k(50) \end{bmatrix} < \begin{bmatrix} k' \\ k' \\ \vdots \\ k' \end{bmatrix} \tag{4.7}$$

$$\begin{bmatrix} -1 & 1 & 0 & \cdots & 0 \\ 0 & -1 & 1 & \cdots & 0 \\ \vdots & \vdots & \vdots & \ddots & \vdots \\ 0 & 0 & \cdots & -1 & 1 \end{bmatrix} \begin{bmatrix} k(1) \\ k(2) \\ \vdots \\ k(50) \end{bmatrix} < \begin{bmatrix} k' \\ k' \\ \vdots \\ k' \end{bmatrix} \tag{4.8}$$

4.2.4   Second Derivative Constraint

To discourage the optimizer from producing stiffness curves that constantly form triangular wave sections at the constraint value $\pm k'$, a constraint was applied to the second derivative of $k(t)$. This constraint also discourages the optimizer from producing sharp peaks, which represent a very fast change in the direction of the stiffness versus time curve. These fast changes in direction are difficult for human joints to do. The shape of these curves also differ from humans in that humans produce smoother, more continuous curves in this context.

Another aspect of these curves that is difficult for humans to achieve is a sustained extreme value. The extreme values that are used as the upper and lower bounds of the optimization, as discussed in section 4.2.2, represent values that humans can achieve for a very short duration. Some of the peaks that resulted from optimizations with only a first derivative restriction involved a relatively slow rise and fall, in a manner that is extremely taxing on human joints and therefore difficult for humans to produce. To avoid these types of results, a second derivative constraint was added, while relaxing the first derivative restriction, to force the optimizer to produce curves that are smoother, but can use the extreme values in more human-like ways.

To apply a second derivative constraint, a similar method was used to the first derivative constraint. Equation 4.9 represents the second derivative of $k(i-1)$, $k(i)$, and $k(i+1)$ being restricted to $\pm k''$.

$$|k(i-1) - 2k(i) + k(i+1)| < k'' \tag{4.9}$$

where k'' represents the constraint value on the second derivative. Similar to with k', it is important to note the dependence of the magnitude of k'' on the magnitude of the time step. Equation 4.9 can then be broken into Equation 4.10 and Equation

4.11.

$$k(i-1) - 2k(i) + k(i+1) < k''$$ (4.10)

$$-k(i-1) + 2k(i) - k(i+1) < k''$$ (4.11)

By the same process as discussed in Section 4.2.3, Equations 4.10 and 4.11 can further be expressed as matrices seen in equations 4.12 and 4.13, respectively.

$$\begin{bmatrix} 1 & -2 & 1 & 0 & \cdots & 0 \\ 0 & 1 & -2 & 1 & \cdots & 0 \\ \vdots & \vdots & \vdots & \vdots & \ddots & \vdots \\ 0 & 0 & \cdots & 1 & -2 & 1 \end{bmatrix} \begin{bmatrix} k(1) \\ k(2) \\ \vdots \\ k(50) \end{bmatrix} < \begin{bmatrix} k'' \\ k'' \\ \vdots \\ k'' \end{bmatrix}$$ (4.12)

$$\begin{bmatrix} -1 & 2 & -1 & 0 & \cdots & 0 \\ 0 & -1 & 2 & -1 & \cdots & 0 \\ \vdots & \vdots & \vdots & \vdots & \ddots & \vdots \\ 0 & 0 & \cdots & -1 & 2 & -1 \end{bmatrix} \begin{bmatrix} k(1) \\ k(2) \\ \vdots \\ k(50) \end{bmatrix} < \begin{bmatrix} k'' \\ k'' \\ \vdots \\ k'' \end{bmatrix}$$ (4.13)

The addition of a second derivative constraint forced the optimizer to avoid sustained spikes towards the boundary values because it would take longer to decrease due to the second derivative being constrained.

4.3   Overall Optimization

The total optimization included all of the constraints listed above and was applied over 1s intervals, which included 50 time steps at $t_{step} = 0.02s$. This can be represented as described in equation 4.14.

$$min \quad f = \sum_{i=1}^{50} (\theta_{NMM}(i) - \theta_{Data}(i))^2$$ (4.14)

$$subject\ to \quad -50Nm \le k(i) \le 100Nm \qquad\qquad i = 1, 2, ..., 50$$

$$|k(i) - k(i-1)| < k' \qquad\qquad i = 2, 3, ..., 50$$

$$|k(i-1) - 2k(i) + k(i+1)| < k'' \qquad\qquad i = 2, 3, ..., 49$$

where $k' = 200Nm$ and $k'' = 2Nm$.

4.4   Notes on Optimizations

The solver used to optimize the discrete stiffness values was Matlab's 'fmincon.' Throughout the optimization process, running the optimizations with different constraints and different initial conditions often lead to curves that included sharp peaks, quick changes, and discontinuities (as discussed in sections 4.2.3 and 4.2.4). The overall goal of these optimizations was to produce a stiffness curve that resembled those that humans might naturally produce [26]. In this pursuit, the various constraints were applied in such a way as to encourage smooth curves with small maximum amplitudes. To do this, the constraint values k' and k'' were gradually decreased until the model's performance began to suffer.

The motivation behind this approach is twofold. Primarily, this type of approach is meant to be a best effort attempt to impose a "biological cost" function onto the stiffness curve, which is meant to emulate the approach that humans take, which is to use the least amount of energy possible. By constraining the magnitude of quick changes in either $k(i)$ or $k'(i)$, it becomes difficult for the optimizer to change direction of $k(i)$ quickly and thus, the resultant curves are smoother and have a smaller average amplitude. The secondary motivation for this approach is that similar to humans, it is analogously advantageous for robots if the stiffness curves that are required are smooth and small in amplitude. Smooth stiffness curves with small amplitude decrease the energy required by the robots to produce a human-like response.

4.5   Variable Damping

During some of the disturbance rejection experimental trials, while the subject was trying to move the handle back to $\theta(t) = 0$, the subject would reach an angle that was close, but not equal, to 0 at which point the subject would prioritize maintaining a constant angular position, rather than moving closer to $\theta(t) = 0$. This deadband region is something of an angular tolerance, θ_{tol}, that the human considers to be "equivalent" to $\theta(t) = 0$. To be more succinct, the subject would reach a region of $-\theta_{tol} < \theta(t) < \theta_{tol}$, and determine that this region was "good

enough" for the task and stop moving closer to $\theta(t) = 0$. This behavior contrasts the behavior of what a robot, as well as the NMM, does in this situation. Due to the non-time-varying characteristic of the control system, the NMM will maintain some torque on the joint until $\theta(t) = 0$.

This difference in behavior between human subjects and the NMM caused difficulties when trying to optimize a stiffness curve in these regions. To compensate for the difference in behavior, damping as a variable quantity was revisited. Although variable damping as compared to variable stiffness is not as effective in changing the general response of the model (see Section 3.2.2), relaxing the damping in situations where the human subjects reached a "good enough" region, allows the model to be more guided by the disturbance and therefore better match the experimental data from the human subjects. To enable the optimizer to control the damping, the constant damping term was broken up into 20 discrete values, one for each interval. The notation used in Equation 4.15 is such that subscripts correspond with interval numbers. The optimizer was allowed to change the damping in a given region in this type of situation. Adding this variable damping term improved the results of the model as compared to the data.

$$
B = \begin{cases} B_1 & 0s \le t \le 1s \\ B_2 & 1s < t \le 2s \\ \quad \vdots \\ B_{20} & 19s < t \le 20s \end{cases} \tag{4.15}
$$

4.6   Results

The optimizations of variable stiffness were successful, ultimately producing 1% of the sum of the squared angular error as compared to a constant stiffness. The optimized stiffness vector $k(i)$ can be seen in Fig. 4.1. The response of the NMM, using the optimized stiffness, well matches the experimental data, as seen in Fig. 4.2, with angular position θ measured in degrees. The vast error reduction between the NMM response with and without a time-varying stiffness provides evidence that a time-varying stiffness has the capacity to significantly improve the NMM response in the context of the disturbance rejection task. Furthermore, the prospect of trying

to recreate this optimized stiffness in real-time by way of a predictive stiffness model was investigated, conducted (see Chapter 5), and tested (see Chapter 6).

Fig. 4.1 demonstrates the optimized stiffness vector k, which varies between high magnitude sections for approximately the first 3s, after which point the magnitude remains within $\pm 1.5 Nm$. The reduction in amplitude seems to indicate that the human subject could learn the general requirements of the task and divert to using less energy to achieve the same response. At the beginning of the disturbance rejection task it seems that the subject had to exert more energy, by way of high magnitude variations in stiffness to establish some stability in the context of the task. The initial high-magnitude response is likely also related to the reflex response of the subject to the task at hand.

It is also important to note that although the stiffness values from the optimization are much higher than typical human stiffness values (but still within the range of possibility), whether or not these values match what the human subject used is not necessarily relevant. The important takeaway is that if a robot were to reproduce these stiffness values, the robot would still mimic human motion behavior. Since these stiffness values are achievable for a robot, this optimized stiffness satisfies the goal of this section, which was to determine a variable stiffness that would enable a robot to reproduce functionally similar motion to humans in the context of the disturbance rejection task.
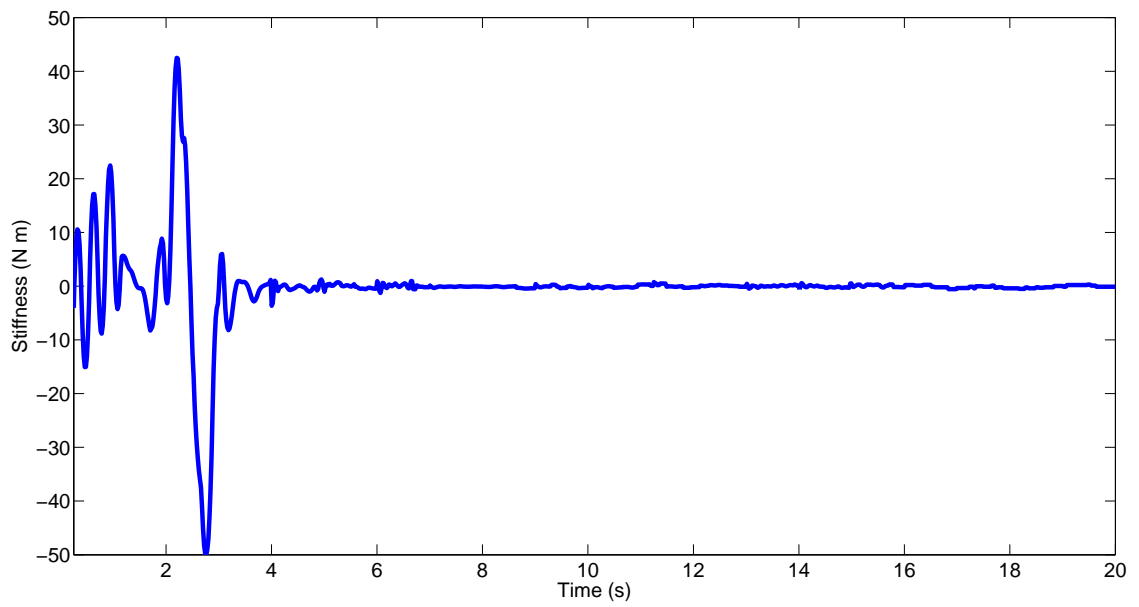
Figure 4.1: Optimized Variable Stiffness Vector (Subject 2, Trial 2)
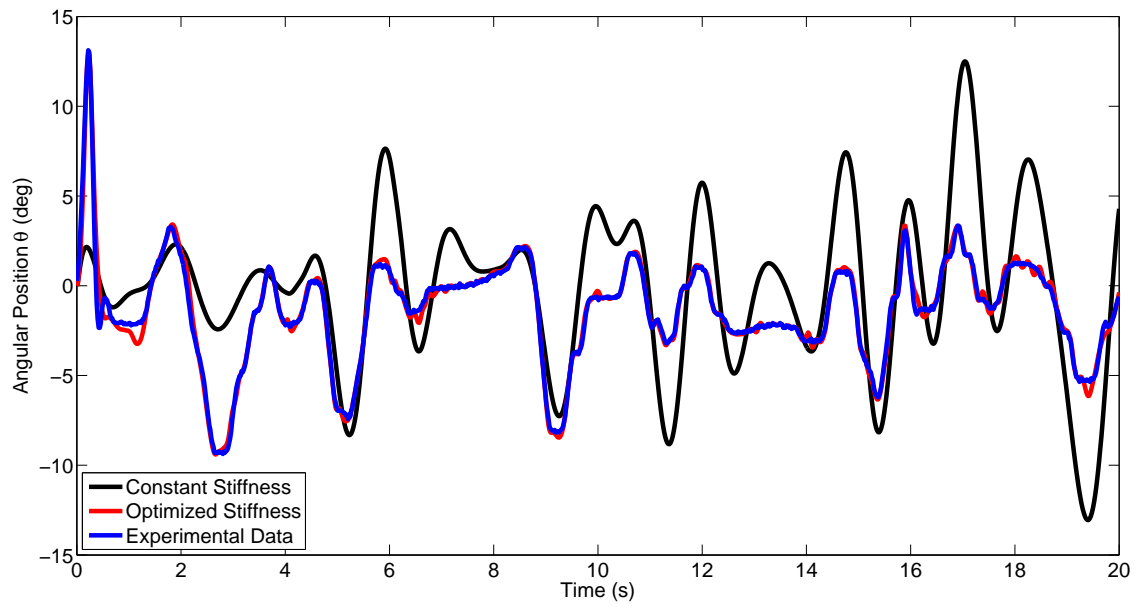
Figure 4.2: NMM Response with Optimized Variable Stiffness (Subject 2, Trial 2)

CHAPTER 5

Predictive Stiffness Models

5.1   Introduction

After a variable stiffness vector $k(t)$ was determined by way of optimization, as described in Chapter 4, a stiffness function was determined using the available input parameters to determine the stiffness value that a human would use for each time step. The predictive stiffness model synthesis represents step 4 of the sequence described in Fig. 1.1, reproduced below as Fig. 5.1. That is, create a $k(\theta, \omega, etc.)$ that would set the stiffness of a variable stiffness joint at any given time, based on the current input parameters, thus reproducing this aspect of human joint motion in a robot.
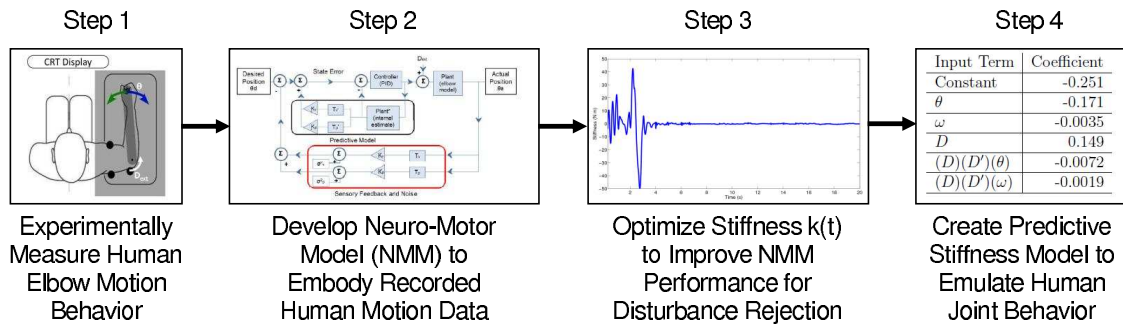
Figure 5.1:   Development Sequence for Predictive Stiffness Model

5.2   Developing the Predictive Stiffness Model

To determine a predictive stiffness function, $k(\theta, \omega, etc)$, the optimized stiffness vector $k(t)$, as determined in Chapter 4, was set as the goal vector while a function k was established with all available system inputs as independent variables. The terms investigated were: constant term (C), disturbance $(D(t))$, disturbance derivative $(D'(t))$, disturbance second derivative $(D''(t))$, angular position $(\theta(t))$, angular velocity $(\omega(t))$, angular acceleration $(\alpha(t))$, angular error $(\theta_{error}(t))$. There were also nonlinear terms that were the product of up to four of these parameters,

including terms exponentiated up to the third power as well. All of the terms were linearly combined to form the initial predictive stiffness function. Using the disturbance as a contributing factor to the stiffness determination is a new idea that has not been used in previous impedance control [14, 20, 22, 31].

Using the Matlab function 'nlinfit,' the coefficients for each of the terms mentioned above were optimized as described in Equation 5.1.

$$min \qquad f = \sum_{i=1}^{1000} (k(\theta(i), \omega(i), etc) - k_{optimized}(i))^2 \qquad (5.1)$$

where $k_{optimized}$ represents the optimized stiffness k, which was determined as described in Section 4.3 and is shown in Fig. 4.1.

After developing an initial model, certain terms that did not significantly affect the output of the function were dropped. Terms that did not cause an average of at least a 3% change in the sum of the squared angular error between the NMM and the experimental data were dropped to avoid unnecessary complexity. To clarify, if a predictive stiffness contained two terms, θ and ω, a term in question, θ, was removed from that predictive stiffness model if it did not meet the requirement described in Equation 5.2.

$$\frac{\sum_{i=1}^{1000} (\theta_{NMM}[k(\theta(i), \omega(i))](i) - \theta_{Data}(i))^2 - \sum_{i=1}^{1000} (\theta_{NMM}[k(\omega(i))](i) - \theta_{Data}(i))^2}{\sum_{i=1}^{1000} (\theta_{NMM}[k(\omega(i))](i) - \theta_{Data}(i))^2} \geq 3\%$$

$$(5.2)$$

where $\theta_{NMM}[k(\theta, \omega)]$ represents the NMM being run with a predictive stiffness model that includes the two terms θ and ω and $\theta_{NMM}[k(\omega)]$ represents the NMM being run with a predictive stiffness model that includes one term ω.

To assess the performance of a given predictive model, the sum of the squared angular error between the model response $\theta(t)$ and the angular position feedback from the experimental data was calculated, as described in Equation 4.1. That error was then compared the sum of the squared angular error that resulted from running the model with a constant stiffness value.

5.3 Initial Predictive Stiffness Models

Predictive stiffness models were developed for the first two trials of data taken from subject two in the disturbance rejection task. The different models that are described below are outlined in Table 5.1. For a discussion of predictive stiffness models with respect to subject one, see Section 5.4.

	Model 1	Model 2	Combined Model
Subject	2	2	2
Trial	1	2	1 and 2

Table 5.1: Predictive Stiffness Models

5.3.1 Model 1

The first resultant stiffness function was based on data from a single trial (subject 2, trial 1). This predictive model resulted in 46% improvement in the squared angular error $(\Sigma(\theta_{model} - \theta_{data})^2)$ of the model performance in a disturbance rejection task relative to a constant, optimized stiffness value. The developed predictive model is a linear combination of the coefficients and terms described in Table 5.2. The performance for this model is shown in Fig. 5.2.

Input Term	Coefficient
Constant	-0.2714 (N m/rad)
θ	-0.0983 (N m/rad^2)
ω	-0.0198 (N m s/rad^2)
α^3	-6.38x10^{-10} (N m s^6/rad^4)
$(D)(D')(\theta)$	0.0029 (s/N m rad^2)
$(D)(D')(\omega)$	0.0035 (s^2/N m rad^2)
$(D)(D')^2$	-0.0024 (s^2/N^2 m^2 rad)

Table 5.2: Predictive Model 1

5.3.2 Model 2

The second resultant stiffness function was based on data from the second trial of data from the same subject as used for Model 1. This predictive model
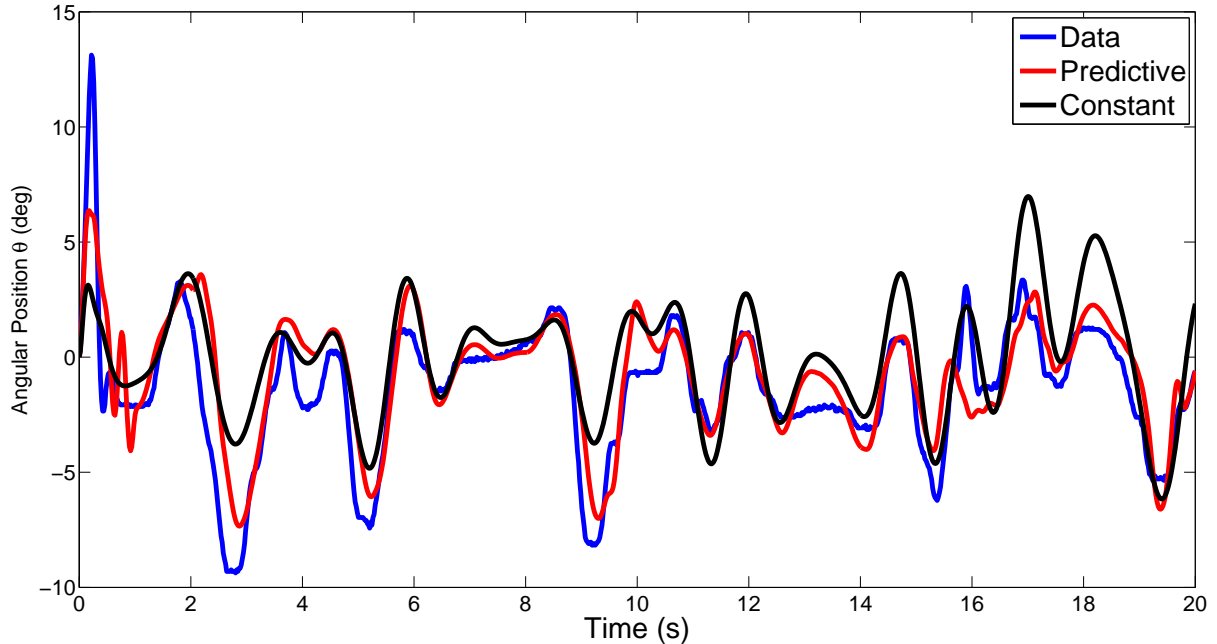
Figure 5.2: Model Performance for Predictive Model 1 (see table 5.2)

resulted in 62% improvement in the squared angular error of the model performance in a disturbance rejection task relative to a constant, optimized stiffness value. The developed predictive model is a linear combination of the coefficients and terms described in Table 5.3. The performance for this model is shown in Fig. 5.3.

Input Term	Coefficient
Constant	-0.222 (N m/rad)
θ	-0.106 (N m/rad^2)
ω	-0.0091 (N m s/rad^2)
α^3	-5.18x10^{-10} (N m s^6/rad^4)
D	0.464 (rad^{-1})
$(D)(D')(\theta)$	-0.0022 (s/N m rad^2)
$(D)(D')(\omega)$	-0.00065 (s^2/N m rad^2)
$(D)(D')^2$	0.0018 (s^2/N^2 m^2 rad)

Table 5.3: Predictive Model 2

5.3.3 Combined Predictive Model

After the successful implementation of the initial predictive stiffness models, a combined, more general model was created by combining the two models. To
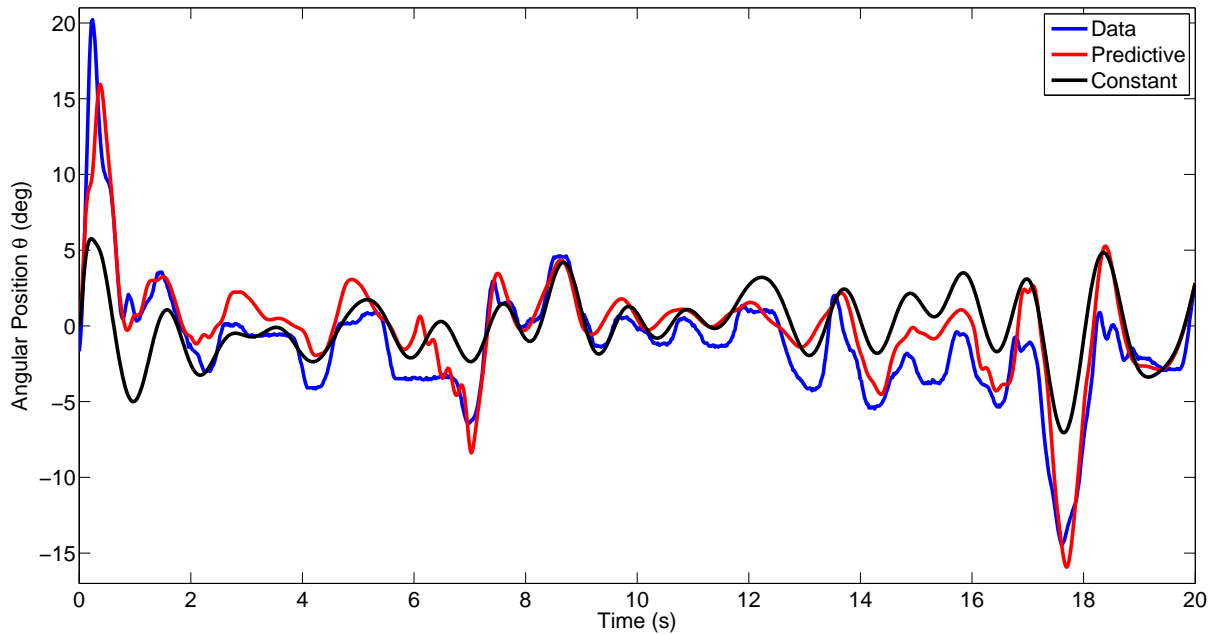
Figure 5.3: Model Performance for Predictive Model 2 (see table 5.3)

combine the two models, the 'nlinfit' command was used, as discussed in Section 5.2. Unlike the way that 'Model 1' and 'Model 2' were developed, the the squared angular error vector that was being minimized was the sum of the angular error vectors that resulted from simulating trial 1 and trial 2. The 'nlinfit' function minimized the combined error of the two trials, thus creating a model that improved the response of both trials, though not as much as the individual models. The combined model resulted in a 27% improvement for the first trial and a 47% improvement for the second trial (Fig. 5.4). While these values are lower than that of the initial two models, the fact that the model works on multiple trials means that it is more general and can be used effectively in a wider context. Furthermore, this model, as seen in Table 5.4, has fewer variables, so it is a less complex model.

5.4   Results and Step Response Discussion

As discussed in Sections 5.3.1, 5.3.2, and 5.3.3, implementing the predictive stiffness model results in substantial improvement between the model response and the experimental data in the context of the disturbance rejection task. Since three of the terms described in Section 5.3.3 include a D dependence, they go to 0 when

Input Term	Coefficient
Constant	-0.251 (N m/rad)
θ	-0.171 (N m/rad^2)
ω	-0.0035 (N m s/rad^2)
D	0.149 (rad^{-1})
$(D)(D')(\theta)$	-0.0072 (s/N m rad^2)
$(D)(D')(\omega)$	-0.0019 (s^2/N m rad^2)

Table 5.4: Combined Predictive Model
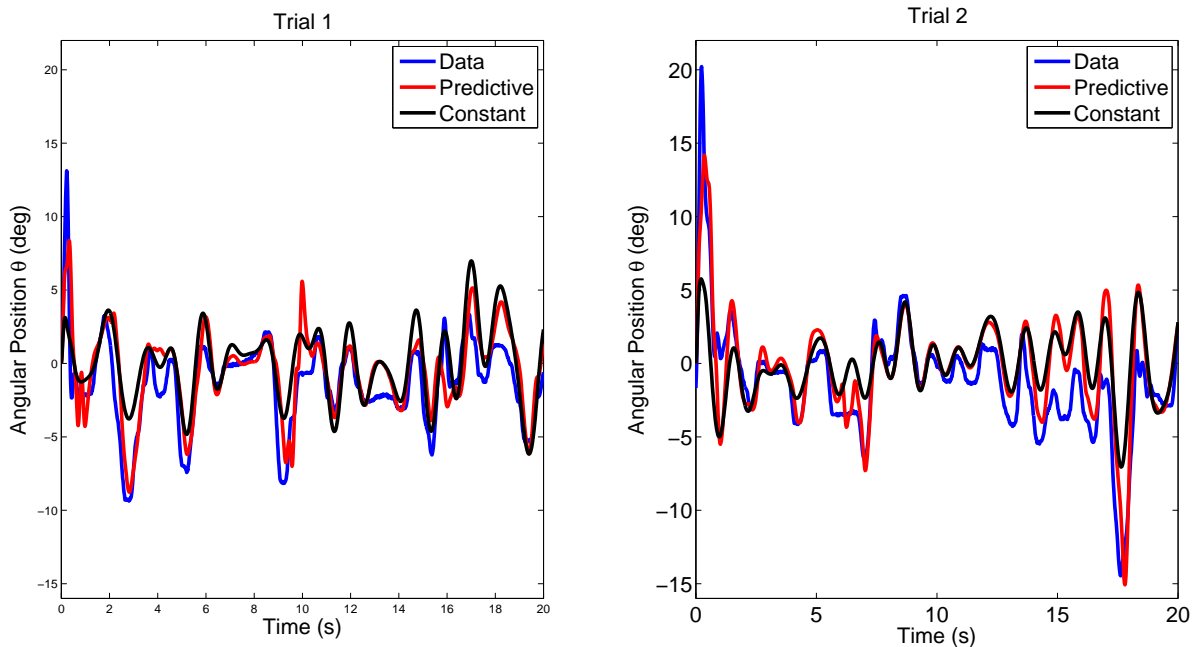
Figure 5.4: Model Performance for Combined Predictive Model (see table 5.4)

$D = 0$, which reduces the complexity of the model when applied to other tasks.

It is important to note also, that for the simulations that were run to assess the performance of the predictive stiffness model, the constant stiffness value was optimized for each respective trial of data. A constant, general value across all trials was not used.

The model improves performance in the context of disturbance rejection, while it maintains the same performance in context of step response. The performance of the predictive stiffness model can be seen in Fig. 5.5, where it is compared to a constant stiffness result. One aspect of the experimental data that the NMM improved on was the higher amplitude peaks. In trial 1, there are higher

amplitude peaks at $t = 0.2s$, $t = 2.6s$, $t = 5.4s$, and $t = 9.1s$, at which points, the predictive model matches the data significantly more than the constant stiffness model does. Similarly, trial 2 has high amplitude peaks at $t = 0.2s$, $t = 7.0s$, and $t = 17.8s$, where again, the predictive stiffness model has a much stronger agreement as compared to the constant stiffness model.
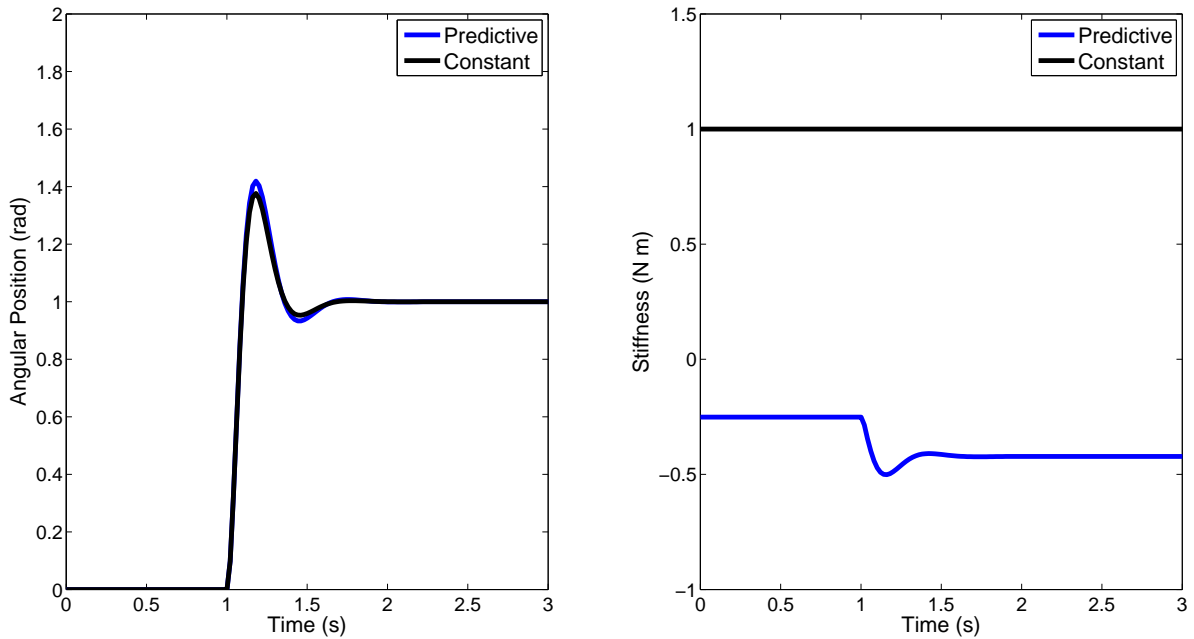
Figure 5.5: Predictive Stiffness Model (see Section 5.3.3) Performance for Step Response

When applied to the data from the other subject of the human subject testing, the combined predictive stiffness model as described in Section 5.3.3 does not demonstrate improvement when compared to a constant, optimized stiffness value. While it does perform well across multiple trials of subject 2, when the model is applied to subject 1, it results in a decrease in performance across an experimental trial of the disturbance rejection task, which can be seen in Fig. 5.6. The predictive stiffness model is stable and the peaks in the angular response have a similar amplitude as compared to the result with a constant stiffness value. It is hypothesized that lack of improvement of the predictive stiffness model is in part due to not having optimized the subject-specific parameters within the predictive stiffness model. The agreement between the NMM with a constant stiffness value and the data is weak and the NMM response, both with and without the predictive

stiffness model, would be improved by a more exhaustive optimization of the subject-specific parameters throughout the NMM.

Another hypothesis of this work is that a more in-depth analysis of each term in the predictive stiffness model could determine which parameters in the predictive stiffness model are subject-specific and which parameters are more general. If the subject-specific parameters of the predictive stiffness model were optimized to the other subject, the predictive stiffness model could improve the NMM response for that subject.
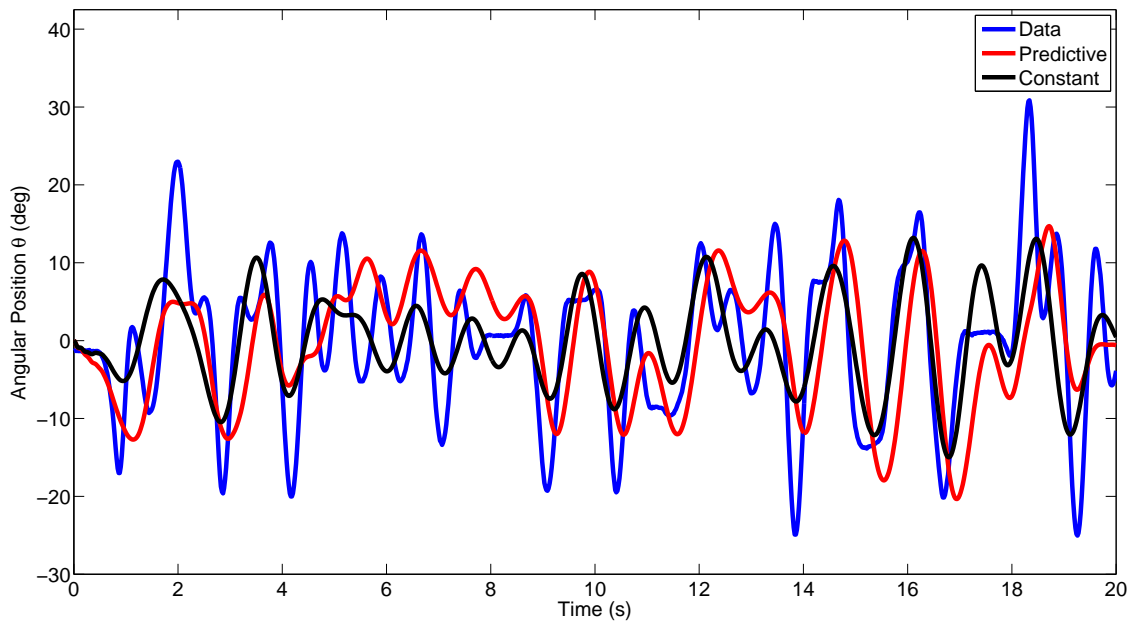
Figure 5.6: Disturbance Rejection Response for Subject 1

Input Term	Units	Model 1	Model 2	Combined
Constant	(N m/rad)	-0.2714	-0.222	-0.251
θ	(N m/rad^2)	-0.0983	-0.106	-0.171
ω	(N m s/rad^2)	-0.0198	-0.0091	-0.0035
α^3	(N m s^6/rad^4)	-6.38x10^{-10}	-5.18x10^{-10}	0
D	(rad^{-1})	0	0.464	0.149
$(D)(D')(\theta)$	(s/N m rad^2)	0.0029	-0.0022	-0.0072
$(D)(D')(\omega)$	(s^2/N m rad^2)	0.0035	-0.00065	-0.0019
$(D)(D')^2$	(s^2/N^2 m^2 rad)	-0.0024	0.0018	0

**Table 5.5:** Comparison of Predictive Model Coefficients

CHAPTER 6

Experimental Verification

6.1   Introduction

In order to verify that the predictive stiffness models described in Sections
5.3.1, 5.3.2, and 5.3.3 respond as theorized by the NMM, an experimental setup was
constructed. This experiment implemented a predictive stiffness model and
performed a step response task and a disturbance response task. The results of the
predictive stiffness model's performance were then compared to both the theoretical
results of the NMM and the experimental results of the motor when run with a
constant stiffness. The goal of the experiment was to verify that the NMM was
producing accurate predictions and to verify that the predictive stiffness model
maintains the same performance as a constant stiffness joint for a step response.
The experimental setup for the step input task involved a 1 DOF Pittman DC
motor, with an 'Advanced Motion Controls' motor driver, connected to Simulink via
a dSPACE 1104 control board. A similar setup was used for the disturbance
rejection task, with the addition of one end of a rubber band held in a constant
position with the other end on the arm, resulting in a sinusoidal torque disturbance
as the plastic arm completed a revolution.

6.1.1   Model Simplifications

Some simplifications to the NMM system had to be made in order to create
an achievable experimental setup. Since there was not a readily available variable
stiffness joint, the predictive stiffness model was implemented via software. This
involved including the predictive stiffness as part of the plant. Since it is not
possible to use a real human elbow, a small plastic pseudo-replica was created by
way of 3D printing and attached to the motor shaft. The combined model,
described in Section 5.3.3, was used for all of the experimental verification discussed
in this chapter and implemented as described in Fig. 6.1.
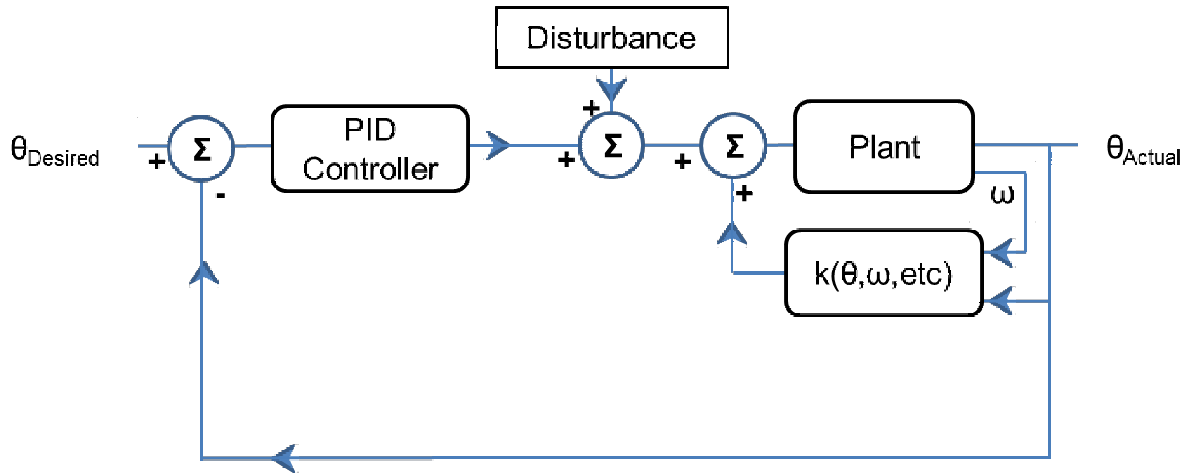
Figure 6.1: Experimental Block Diagram for Controlled Motor

The motor and "forearm" were modeled as mass-damper system, with the predictive or constant stiffness term being included as part of the plant, as described in Fig. 6.1 [32]. Note that the same transfer function was used with a constant stiffness, with the k being set to a constant $k = 1Nm$. The overall plant transfer function for the system can be reduced to be written as shown in Equation 6.1.

$$G(s) = \frac{1}{Js^2 + Bs + k(\theta, \omega, etc.)} \tag{6.1}$$

6.1.2 Controller

In the context of the NMM, a PID controller was determined to best match the human control system [1,27]. However, for the experimental setup described above, a PD controller was determined by manual tuning to ensure stability of the motor-mass system, where P = 0.8 and D = 0.6. This was maintained throughout all experimental cases described below.

Section 4.2 discusses the change of the time step used in the NMM from 0.001s to 0.02s. In this experimental setup, the time step was changed to match the motor controller's limit of 0.0001 s. Reducing the time step allowed the controller to react much quicker than when the system was tested in simulation with the time
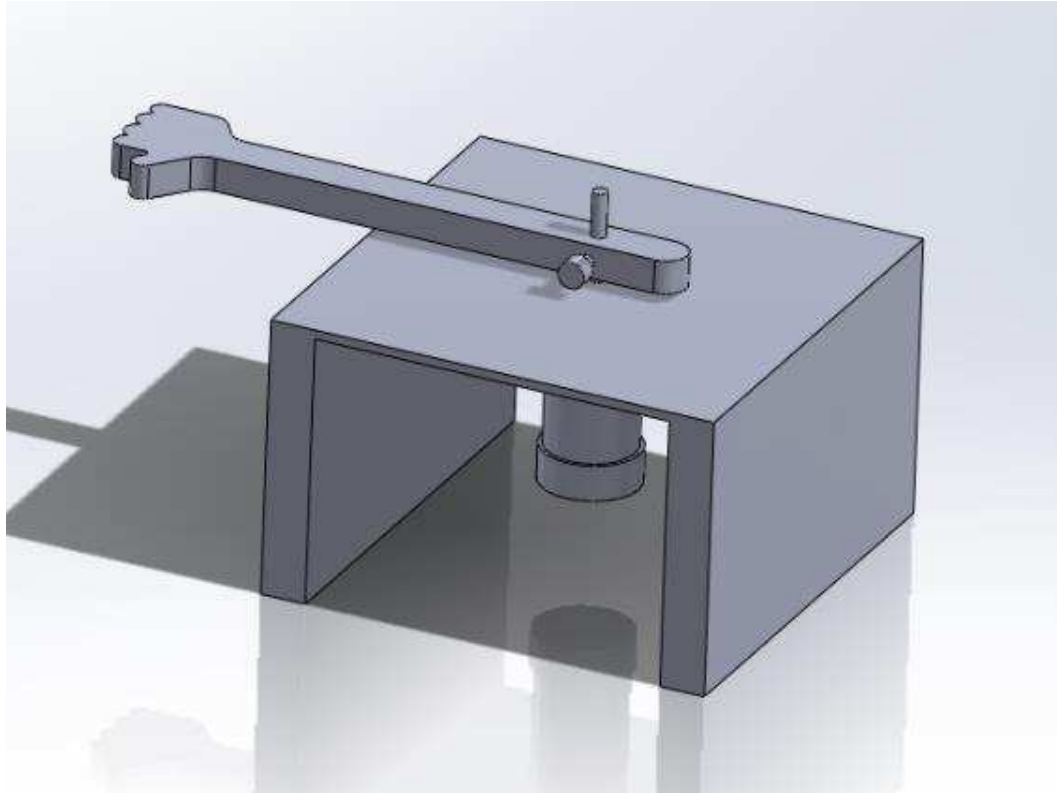
Figure 6.2: Experimental Step Response Setup

step of 0.02s. This change enables the system to be treated as quasi-static when rotated at slow speeds.

6.2 Experimental Tasks and Results

To verify that the physical implementation of the predictive stiffness model works as expected, it was run through the two tasks that the work in this thesis focused on: step input and disturbance rejection. Prior to experimentally running these tasks, simulated results were obtained from the NMM, which had been modified to include the plant and controller described in Section 6.1.1. These results were compared to the experimentally obtained results described below to verify that the predictive stiffness model would function in the ways predicted by simulation.

The predictive stiffness model had been developed with coefficients with specific units, as described in Section 5.3. Since the experimental setup had a plant with different components such as motor inertia, plastic part inertia, and current-to-torque conversion factor for the motor controller, the relative magnitudes
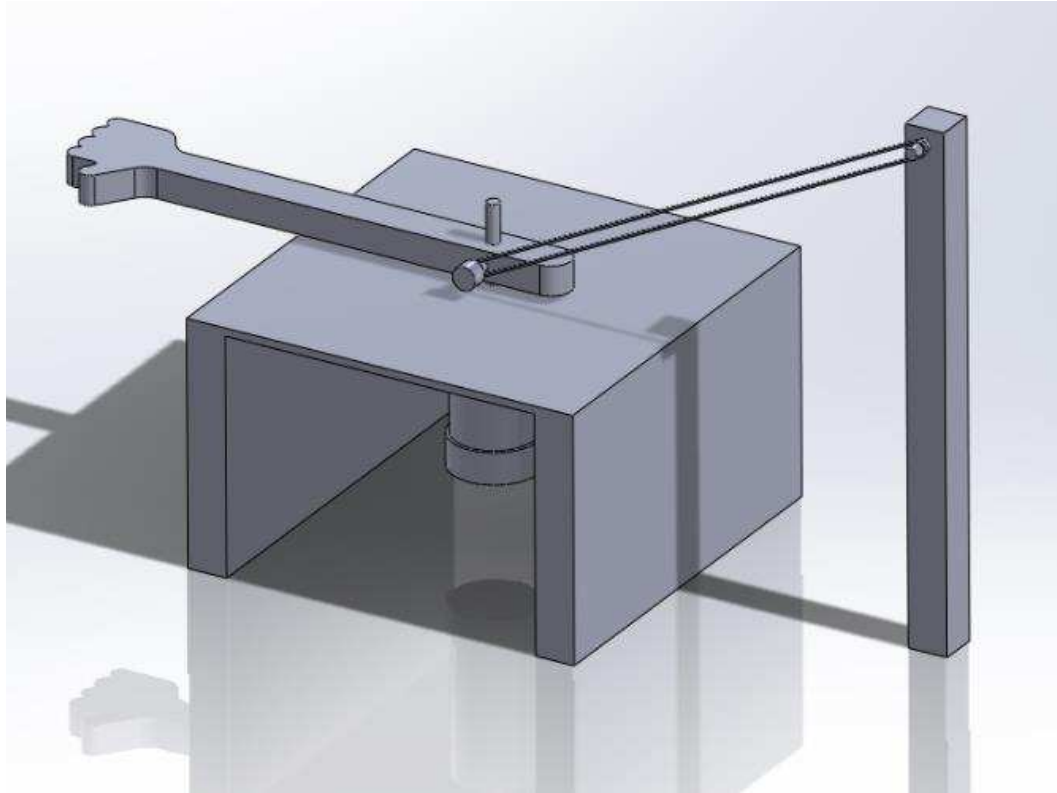
Figure 6.3: Experimental Disturbance Rejection Setup

of the PID control signal and the predictive stiffness model are lost. To properly reproduce the same relative magnitudes, gain blocks were placed in front of the controlled signal and the output of the predictive stiffness model to reproduce consistent relative magnitudes as appeared in simulation.

6.2.1 Step Response

A step input task was performed with the experimental setup seen in Fig. 6.2. The step size used was approximately 20 degrees, which is approximately consistent with the order of magnitude of oscillations present in the human subject tasks described in Section 2.3. As predicted by the NMM (as described in Fig. 5.5) the predictive stiffness model results in a similar performance as compared to a constant stiffness (k=1.2 N m, which is typical for the human elbow [30]). This was experimentally verified as seen in Fig. 6.4.

6.2.2   Disturbance Rejection

As discussed in Section 2.6.2, disturbance rejection was a large focus of this work. Consequently, disturbance rejection was an important aspect of the predictive stiffness model to verify. Due to the scope of this project, an extensive disturbance rejection test was not possible. The test performed involved using a rubber band, with known elastic properties (spring constant = 18.27 N/m), connected to the moving mass and held at a constant distance as shown in Fig. 6.3. The NMM was given a constant, slow velocity while run directly through the dSPACE control board. The slow velocity ($\omega = 0.2rad/s$) was used so that the system could be treated as quasi-static. The rotation caused the rubber band to apply a sinusoidal torque disturbance (see Equation 6.2) as the mass rotated fully around the motor.

$$D(t) = -0.4cos(4\pi t/30 + 1)Nm \qquad (6.2)$$

Since the disturbance was a relatively low torque (0.4 N m) the predictive
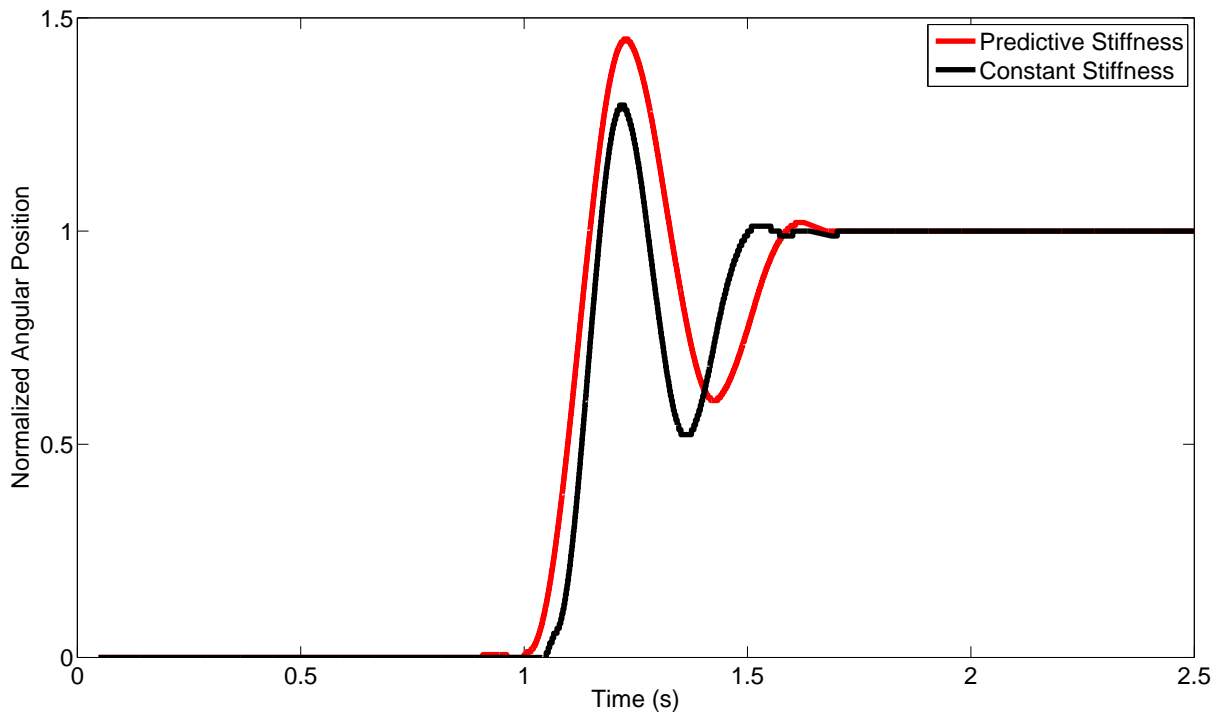
Figure 6.4:   Experimental Step Response with Predictive and Constant Stiffness

stiffness model was expected to remain closer to $\theta = 0$ as compared to the constant stiffness model. This expectation was experimentally verified and the results of the disturbance rejection experimental task are displayed in Fig. 6.5, in which θ is measured in radians. The experimental data presented in Fig. 6.5 represents the desired position, which was a slow, constant, and positive angular velocity, subtracted from the measured angular position θ and then normalized. This operation causes the desired trajectory to appear in the plot as $\theta(t) = 0$, which enabled the predicted and measured results to be displayed simultaneously in a meaningful way.
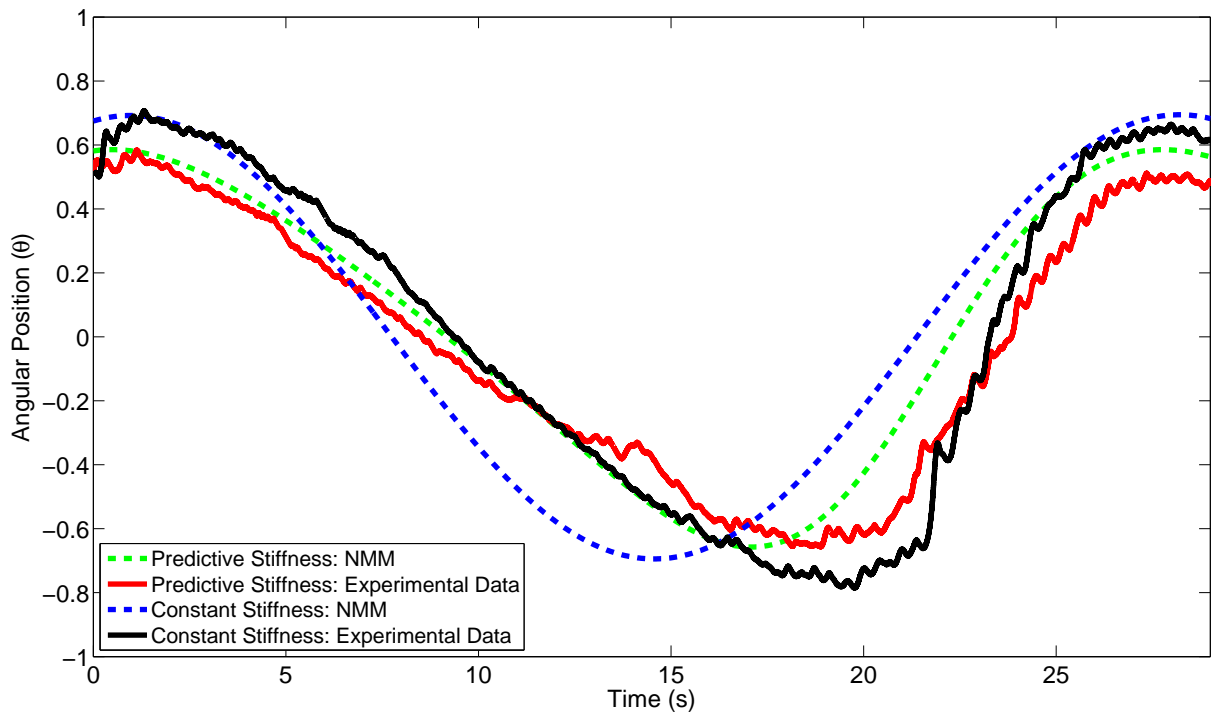
Figure 6.5: Experimental Disturbance Rejection with Predictive and Constant Stiffness

6.3   Conclusion

The first goal of the experimental testing was to verify that the the NMM response for a step input task is similar for constant stiffness as compared to predictive stiffness, as shown in Fig. 5.5. Fig. 6.4 demonstrates agreement between the step response for constant stiffness and step response for predictive stiffness.

The second goal of this experimental test was to test agreement between the theoretical output of the NMM in simulation and experimental data in the context of a disturbance rejection task. Fig. 6.5 displays agreement between the experimental and simulated results for predictive and constant stiffness. As expected, the predictive stiffness improves the NMM response in the context of a disturbance rejection task.

Many industrial robots are rigid to the point where small disturbances do not affect the response of the robot. Some robots can maintain a commanded position even when a 300 N m disturbance is applied [33]. Since this experimental setup is affected by the disturbance, as expected by the NMM, despite the magnitude of the disturbance being only 0.4 N m, it can be stated that a robot that uses this predictive stiffness model will demonstrate motion that is more human-like as compared to an industrial robot that would remain unaffected by such a disturbance.

While this testing was not meant to be overly thorough and definitive, the results substantiate the idea that a robot using this type of joint would demonstrate the human-like characteristics that are present in the NMM. It is also useful to note that the experiment verifies the idea that the predictive stiffness model can be implemented purely with software, as opposed to with hardware via a variable stiffness joint, if desired. Implementing the predictive stiffness model with software would enable existing robots to use this to move in a more human-like manner, without requiring hardware changes.

CHAPTER 7

Conclusions, Future Work, and Potential Applications

The main motivation for this research, as mentioned in Section 1.1, was to engineer robotic joints that demonstrate functionally similar motion to humans. To create these joints, human motion was directly observed and modeled. A model for a robot to properly emulate human motion behavior was developed. The ability to produce human-like motion allows a robot to be the "best of both worlds." That is, a robot that uses this model would demonstrate the strengths of robot motion, such as accuracy and repeatability, while not exhibiting the negative aspects of robotic motion such as high power requirements and overly stiff movements.

The sequence described in Fig. 1.1 was successfully demonstrated. Human subject data was used, in conjunction with the neuro-motor model (NMM) developed by Beardsley, et al., to optimize a time-varying stiffness vector [1]. The optimized time-varying stiffness vector was used as a goal for an optimized function $k(\theta, \omega, etc.)$, which was synthesized as described in Chapter 5. The predictive stiffness model presented in Section 5.3.3 successfully improved the response of the NMM in the context of the disturbance rejection task described in Section 2.3 over multiple trials of one human subject. The predictive stiffness model was also demonstrated experimentally in the context of a step input task and a disturbance rejection task.

This work developed a predictive stiffness model designed to enable a robot to reproduce the stiffness value that a human would use in a given situation. The predictive stiffness model is a function that attempts to use angular position (θ), angular velocity (ω), angular acceleration (α), disturbance (D), and disturbance derivative (D') as inputs in the same manner as humans in order to produce human-like stiffness values and thereby human-like motion. If this predictive stiffness model were implemented in a robot, that robot would have the capability to move in a more human-like manner as compared to current robots.

If this predictive stiffness model were to be implemented with a variable stiffness joint, the negative stiffness, as discussed in Section 4.2.2, would have to be eliminated. To eliminate negative stiffness, the predictive stiffness model would have to be modified to produce only positive stiffness values and then also include a way for the predictive stiffness model to modify the controlled signal to switch the sign when appropriate.

7.1   Limitations of the Predictive Stiffness Model

One current limitation of the predictive stiffness model is a failure to improve performance when applied to additional subjects, as described in Section 5.4. If this predictive stiffness model were to be implemented, it would have to be made to be more robust with respect to different subjects. A further study of the terms in the predictive stiffness model could isolate the significance of each term and identify which terms need to be optimized to individual subjects. This type of investigation could also lead to an understanding of how to modify terms to achieve different "flavors" of motion, depending on what is desired. Ideally, the predictive stiffness model would perform well in the context of different subjects and potentially in the context of different robot dynamics as well.

7.2   Potential Applications

There are many applications in which humans and robots share an environment and these environments would be ideal for a robot that could properly emulate human motion. Applications like these include assembly lines, in-home robotics, robot-driven physical therapy machines, powered prostheses, and neuro-implant-controlled robots.

7.2.1   Collision Avoidance

By engineering robotic joints that embody human motion, humans that encountered this robot would be better prepared to avoid collisions with it. Since humans have an internal model of human motion, the brain often expects human motion [34]. Since the brain expects human motion, which is smooth and continuous, often the abrupt and stiff movements of robots can be hard to

anticipate for humans. When the motion of a moving body is hard to anticipate, it becomes more likely that when interacting with such a robot, that a human would have a hard time avoiding the trajectories that the robot is following. By implementing a predictive stiffness model into a robot, the robot would move in a more smooth and human-like manner. Since the robot would be moving in a more human-like manner, it would be easier for a human to anticipate the movements of the robot, which would enable the human to avoid potential collisions because the human could predict the location of the robot in the future with more accuracy.

7.2.2   In-Home Robotics

One of the major differences between a robot that were to adopt the predictive stiffness model described in section 5.3.3 and current robots is the behavior in the context of a collision. Many current robots, which were designed for industrial use, maintain a high stiffness value to enable rigid, repeatable motion. The motion behavior of these robots in the context of a collision with a human is therefore dangerous. Since the stiffness is so high, these robots do not yield at any point in a collision. If a human is in the way of the path of the robot, it will "power" through, which can cause severe injuries to a human. A robot exhibiting the variable stiffness characteristics as described in Section 5.3.3 would have a much lower stiffness in general and furthermore would adapt the stiffness to be lower if a collision were to begin due to stiffness being a function of any input disturbance. By having a much lower stiffness in the context of a collision, such a robot would yield much more than typical robots would and therefore be much safer for a human that might collide with a robot. This characteristic would be important for in-home robotics, due to the heavily chaotic nature of a home environment.

7.2.3   Assembly Lines

Since the predictive stiffness model described in Section 5.3.3 is made up of gains multiplied by input parameters, it would be possible to adjust these gains to determine the level at which the model is applied. By turning all gains except that of the constant term (as described in Table 5.4), down to 0, the model could be reduced to a constant stiffness value, which is typical of industrial robots. Being

able to vary between moving as a human-like robot and a stiff, industrial robot would enable robots used in industrial automation to serve a twofold purpose: work as fast, stiff, and efficient robots when human "collaborators" are not present and work as cooperative, human-like robots when humans are present. This type of situation could be instituted with a safety light curtain as described in Fig. 7.1.
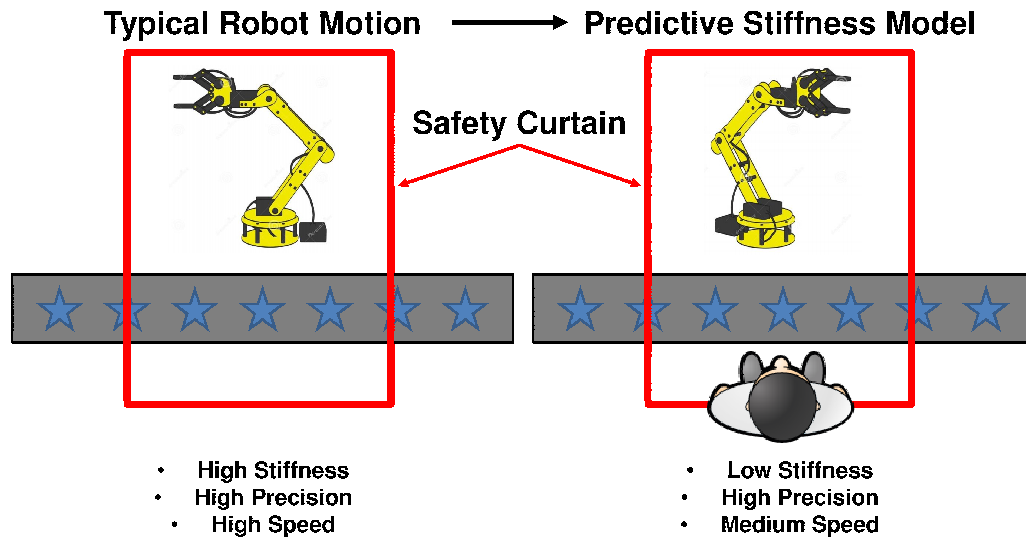
Figure 7.1: Robot Assembly Line Behavior Transition

7.2.4 Robot Personalities

Similar to the way that the model gains could be varied to achieve different types of robot motion as described in Section 7.2.3, these gains could be adjusted to achieve different types of human motion. Future work in this area of research could attempt to isolate correlations between aspects of the predictive stiffness model and human body/motion types, which could enable different "personalities" that a robot could adopt depending on the specific type of human motion that a user wanted.

7.3 Future Work

The first project that presents itself from this work would be a rigorous implementation of the predictive stiffness model described in Section 5.3.3. Variable stiffness joints have been demonstrated, as described in Section 1.2. To fully implement this model in the context of a robot, inertial bodies that match those of humans (used in the plant dynamics described in Section 2.4.4) would have to be

manufactured, which could be done with 3D printing to achieve the precise inertial properties, or with more traditional manufacturing methods. A generic PID controller would be able to implement the controller described in Section 2.4.1, provided it could achieve gains of the proper order of magnitude. A sensing system composed of encoders and torque sensors would be able to properly measure the required input parameters necessary for the predictive stiffness model.

If one were to implement the predictive stiffness model, there might be the concern that since the model has to take time to predict the stiffness value, that computing and sensing delays may be too severe and may limit the performance of the model. However, it is important to note that a time step of $t = 0.02s$ was used throughout the simulation of the NMM and the system performed well in that context. In actuality, control and sensing systems typically work on the order of 1,000 Hz or 10,000 Hz, which would be much faster than the time step used in this work. This would mean that, if properly implemented, the predictive model would function at least as well as documented in Section 5.4. Realistically, the predictive stiffness model would no longer be artificially delayed by 0.02s throughout the simulations, but rather would respond much faster.

Human-robot interaction (HRI) as a field is a growing subset of robotics. As many of the applications described above become more prominent, the desire for humans and robots to be able to cooperate well increases. Some possibilities for future work that stem from the work presented in this thesis include investigating time-varying damping, developing variable stiffness joints to properly implement the predictive stiffness models described in this thesis, and extrapolating the capabilities of a joint that demonstrates this predictive stiffness model to a high DOF robot that can fully move in a more human-like manner as compared to many current robots.

One of the more significant areas of research that was out of the scope of the work in this thesis is trying to understand the significance of each of the terms of the predictive stiffness model described in 5.3.3. Presumably, by changing the gains for different terms, a robot using that model would change it's movement behaviors. Such a robot could move between acting more rigid, like typical industrial robots, and acting more compliant, more like humans. The significance of these terms would further play a role in using multiple predictive stiffness joints to create a

robot, where different joints, such as the knee joints, would potentially require different parameters as compared to those used for a wrist joint. Furthermore, different parameters could correspond to different types of motion among humans. A better understanding of this concept should be able to shine some light on the differences between the predictive stiffness model's performance when compared between subjects (see Section 7.1).

Ultimately, a deeper understanding of the specific terms associated with the predictive stiffness model would open many doors for interesting research projects. The work presented in this thesis has hopefully augmented the understanding of how humans vary stiffness when performing different motion tasks and would enable the development of a robot that could demonstrate improved performance in the context of disturbance rejection.

REFERENCES

[1] Megan L Heenan, Robert A Scheidt, and Scott A Beardsley. Visual and proprioceptive contributions to compensatory and pursuit tracking movements in humans. In *Engineering in Medicine and Biology Society, EMBC, 2011 Annual International Conference of the IEEE*, pages 7356–7359. IEEE, 2011.

[2] RJ Peterka. Sensorimotor integration in human postural control. *Journal of Neurophysiology*, 88(3):1097–1118, 2002.

[3] Masaki Togai and Osamu Yamano. Analysis and design of an optimal learning control scheme for industrial robots: A discrete system approach. In *Decision and Control, 1985 24th IEEE Conference on*, volume 24, pages 1399–1404. IEEE, 1985.

[4] C Cosner, G Anwar, and M Tomizuka. Plug in repetitive control for industrial robotic manipulators. In *Robotics and Automation, 1990. Proceedings., 1990 IEEE International Conference on*, pages 1970–1975. IEEE, 1990.

[5] Dongheui Lee, Christian Ott, and Yoshihiko Nakamura. Mimetic communication model with compliant physical contact in humanhumanoid interaction. *The International Journal of Robotics Research*, 29(13):1684–1704, 2010.

[6] Michael Zinn, Oussama Khatib, Bernard Roth, and J Kenneth Salisbury. Playing it safe [human-friendly robots]. *Robotics & Automation Magazine, IEEE*, 11(2):12–21, 2004.

[7] Tamim Asfour and Rüdiger Dillmann. Human-like motion of a humanoid robot arm based on a closed-form solution of the inverse kinematics problem. In *Intelligent Robots and Systems, 2003.(IROS 2003). Proceedings. 2003 IEEE/RSJ International Conference on*, volume 2, pages 1407–1412. IEEE, 2003.

[8] Oussama Khatib, Luis Sentis, Jaeheung Park, and James Warren. Whole-body dynamic behavior and control of human-like robots. *International Journal of Humanoid Robotics*, 1(01):29–43, 2004.

[9] Sebastian Wolf and Gerd Hirzinger. A new variable stiffness design: Matching requirements of the next robot generation. In *Robotics and Automation, 2008. ICRA 2008. IEEE International Conference on*, pages 1741–1746. IEEE, 2008.

[10] Alin Albu-Schäffer, Sami Haddadin, Ch Ott, Andreas Stemmer, Thomas Wimböck, and Gerd Hirzinger. The DLR lightweight robot: Design and control concepts for robots in human environments. *Industrial Robot: An International Journal*, 34(5):376–385, 2007.

[11] Auke Jan Ijspeert, Jun Nakanishi, and Stefan Schaal. Movement imitation with nonlinear dynamical systems in humanoid robots. In *Robotics and Automation, 2002. Proceedings. ICRA'02. IEEE International Conference on*, volume 2, pages 1398–1403. IEEE, 2002.

[12] Shinichiro Nakaoka, Atsushi Nakazawa, Kazuhito Yokoi, Hirohisa Hirukawa, and Katsushi Ikeuchi. Generating whole body motions for a biped humanoid robot from captured human dances. In *Robotics and Automation, 2003. Proceedings. ICRA'03. IEEE International Conference on*, volume 3, pages 3905–3910. IEEE, 2003.

[13] Nancy S Pollard, Jessica K Hodgins, Marcia J Riley, and Christopher G Atkeson. Adapting human motion for the control of a humanoid robot. In *Robotics and Automation, 2002. Proceedings. ICRA'02. IEEE International Conference on*, volume 2, pages 1390–1397. IEEE, 2002.

[14] Neville Hogan. Impedance control: An approach to manipulation. In *American Control Conference, 1984*, pages 304–313. IEEE, 1984.

[15] Neville Hogan. Impedance control of industrial robots. *Robotics and Computer-Integrated Manufacturing*, 1(1):97–113, 1984.

[16] Neville Hogan. Impedance control: An approach to manipulation: Part II implementation. *Journal of dynamic systems, measurement, and control*, 107(1):8–16, 1985.

[17] Neville Hogan. Controlling impedance at the man/machine interface. In *Robotics and Automation, 1989. Proceedings., 1989 IEEE International Conference on*, pages 1626–1631. IEEE, 1989.

[18] J Edward Colgate. Robust impedance shaping telemanipulation. *Robotics and Automation, IEEE Transactions on*, 9(4):374–384, 1993.

[19] Alin Albu-Schäffer, Christian Ott, and Gerd Hirzinger. A unified passivity-based control framework for position, torque and impedance control of flexible joint robots. *The International Journal of Robotics Research*, 26(1):23–39, 2007.

[20] Junho Choi, Sunchul Park, Woosub Lee, and Sung-Chul Kang. Design of a robot joint with variable stiffness. In *Robotics and Automation, 2008. ICRA 2008. IEEE International Conference on*, pages 1760–1765. IEEE, 2008.

[21] Sami Haddadin, Michael Weis, Sebastian Wolf, and Alin Albu-Schäffer. Optimal control for maximizing link velocity of robotic variable stiffness joints. In *IFAC World Congress*, pages 6863–6871, 2011.

[22] Giovanni Tonietti, Riccardo Schiavi, and Antonio Bicchi. Design and control of a variable stiffness actuator for safe and fast physical human/robot interaction. In *Robotics and Automation, 2005. ICRA 2005. Proceedings of the 2005 IEEE International Conference on*, pages 526–531. IEEE, 2005.

[23] Aaron Steinfeld, Terrence Fong, David Kaber, Michael Lewis, Jean Scholtz, Alan Schultz, and Michael Goodrich. Common metrics for human-robot interaction. In *Proceedings of the 1st ACM SIGCHI/SIGART conference on Human-robot interaction*, pages 33–40. ACM, 2006.

[24] Markus Grebenstein and Patrick van der Smagt. Antagonism for a highly anthropomorphic hand–arm system. *Advanced Robotics*, 22(1):39–55, 2008.

[25] Antonio Bicchi and Giovanni Tonietti. Fast and "Soft-arm" tactics. *Robotics & Automation Magazine, IEEE*, 11(2):22–33, 2004.

[26] DJ Bennett, JM Hollerbach, Y Xu, and IW Hunter. Time-varying stiffness of human elbow joint during cyclic voluntary movement. *Experimental Brain Research*, 88(2):433–442, 1992.

[27] Chintan Poladia. Systems identification of sensorimotor control for visually guided wrist movements. Master's thesis, Marquette University, Milwaukee, WI, 2009.

[28] RC Miall, DJ Weir, DM Wolpert, and JF Stein. Is the cerebellum a Smith predictor? *Journal of Motor Behavior*, 25(3):203–216, 1993.

[29] RF Chandler, CE Clauser, JT McConville, HM Reynolds, and JW Young. Investigation of inertial properties of the human body. Technical report, DTIC Document, 1975.

[30] JN Howell, G Chleboun, and R Conatser. Muscle stiffness, strength loss, swelling and soreness following exercise-induced injury in humans. *The Journal of physiology*, 464(1):183–196, 1993.

[31] Shane A Migliore, Edgar A Brown, and Stephen P DeWeerth. Biologically inspired joint stiffness control. In *Robotics and Automation, 2005. ICRA 2005. Proceedings of the 2005 IEEE International Conference on*, pages 4508–4513. IEEE, 2005.

[32] Joseph V Prisco and Philip A Voglewede. A dynamic model of a belt driven electromechanical xy plotter cutter. In *ASME 2012 International Design Engineering Technical Conferences and Computers and Information in Engineering Conference*, pages 1459–1463. American Society of Mechanical Engineers, 2012.

[33] A Zalucky and DE Hardt. Active control of robot structure deflections. *Journal of dynamic systems, measurement, and control*, 106(1):63–69, 1984.

[34] Randolph Blake and Maggie Shiffrar. Perception of human motion. *Annu. Rev. Psychol.*, 58:47–73, 2007.